An Air–Sea Interaction Theory for Tropical Cyclones. Part II: Evolutionary Study Using a Nonhydrostatic Axisymmetric Numerical Model

RICHARD ROTUNNO

National Center for Atmospheric Research, Boulder, CO 80307*

KERRY A. EMANUEL

Center for Meteorology and Physical Oceanography, Massachusetts Institute of Technology, Cambridge, MA 02139

(Manuscript received 17 April 1986, in final form 17 September 1986)

ABSTRACT

In Part I of this study an analytical model for a steady-state tropical cyclone is constructed on the assumption that boundary-layer air parcels are conditionally neutral to displacements along the angular momentum surfaces of the hurricane vortex. The reversible thermodynamics implied by this assumption allows the mature storm to be thought of as a simple Carnot engine, acquiring heat at the high-temperature ocean surface and losing heat near the low-temperature tropopause. Although the oceanic heat source is universally recognized as the *sine qua non* for the mature hurricane, there is also wide acceptance of conditional instability of the second kind (CISK) (which makes no specific reference to surface heat fluxes) as the formative mechanism. This ambivalence is seen in that all numerical-simulation studies find it essential to have transfer from the ocean surface yet all start from a conditionally unstable atmosphere. The hypothesis put forward in Part I, based on the steady-state theory, is that the truly important thermodynamic interaction, *even in the developing stage*, is between vortex and ocean (as distinct from vortex and convection sustained by preexisting conditional instability as in the CISK theory) with cumulus convection rapidly redistributing heat acquired at the oceanic source upward and outward to the upper tropospheric sink. On this view, it is not the organization of convection that is needed per se, but the organization of surface heat flux. We have constructed a time-dependent nonhydrostatic axisymmetric numerical model with convection explicitly accounted for to examine this idea. The numerical experiments show that as a result of a finite-amplitude air–sea interaction instability a hurricane-like vortex may indeed amplify in an atmosphere which is neutral to cumulus convection and attain an intensity and structure which are in excellent agreement with the theoretical predictions of Part I. We examine in detail the model's heat budget which confirms the crucial importance of boundary-layer processes in controlling the structure and evolution of the vortex. We also confirm the conjecture made in Part I that, within a large-scale limit, the horizontal size of the mature tropical cyclone is determined by that of the initial disturbance.

1. Introduction

Early theoretical studies of tropical cyclones focused almost exclusively on the dynamics of moist convection (see the review by Yanai, 1964). This early work suffered from the result that disturbances of the smallest horizontal scale should amplify most rapidly and so could not explain the scale of the cyclones. Charney and Eliassen (1964), among others, recognized this defect and proposed that the secondary circulation (Ekman pumping) of an incipient large-scale vortex could organize the small-scale, otherwise randomly distributed cumulus clouds into the finite-size area near the center of the vortex. The convection thus organized would then act as a finite-size heat source at the vortex center and consequently intensify it. The stronger secondary circulation of the intensified vortex would then advectively import the moisture needed for continued convection which would further intensify the vortex, and so on. This process was termed conditional instability of the second kind (CISK). Observations show, however, that there are anomalously large values of equivalent potential temperature, θ_e (moist entropy), in the hurricane boundary layer, which no amount of convergence could account for in the absence of a source, and without which it would be impossible to explain the magnitude of the low central pressure in the tropical cyclone (Malkus and Riehl, 1960). That source is the tropical ocean, as originally suggested by Riehl (1954, p. 287) and demonstrated convincingly by Ooyama (1969) in his numerical simulation. The anomalous heat flux from the ocean to the atmosphere is due to both high winds, which increase the transfer rate, and low pressure, which increases the saturation equivalent potential temperature of the sea surface. In Part I (Emanuel, 1986) of this study, it is argued that, in view of these facts, the CISK mechanism overemphasizes, as did the early research, the role played by cumulus convection since the really important inter-

* The National Center for Atmospheric Research is sponsored by the National Science Foundation.

action is between the developing vortex and the exchanges at the sea surface, with cumulus clouds merely redistributing upward the extra latent heat acquired at the surface.

In that paper a steady-state nonlinear model for the tropical cyclone is constructed under the assumption of conditional neutrality of boundary-layer air to displacements along surfaces of constant angular momentum. This assumption, along with the assumptions of hydrostatic and gradient wind balance, allows several specific relations to be developed which are in agreement with the available evidence. More important, the reversible thermodynamics implied in the conditional-neutrality assumption allows the hurricane to be thought of as a simple Carnot engine acquiring heat from the high-temperature ocean reservoir while losing heat at low temperature in the upper troposphere. (This basic idea was adumbrated by Riehl, 1954, p. 322; and summarized recently by Ooyama, 1982, but, to our knowledge, no quantitative predictions based on it had been made.) This is a steady-state model, and so it is organically incapable of describing the development of the vortex with time. Nonetheless, it is conjectured in Part I that the development of the vortex may likewise take place under nearly neutral conditions with each additional increment of latent heat put in by the ocean almost immediately redistributed upward in cumulus clouds. In particular, we are led to inquire whether *any* latent instability beyond that needed to overcome internal dissipation within cumulus clouds is required.

Because all existing numerical simulations of tropical cyclones begin with very unstable soundings, the answer to this question is not available in the literature. To help find an answer to this and other related questions raised in Part I, we have developed a time-dependent, nonhydrostatic, axisymmetric numerical model with convection explicitly accounted for. The model is of the general type developed by Klemp and Wilhelmson (1978, hereinafter KW) for the study of cumulus clouds, and adapted by Willoughby et al. (1984) for the study of tropical cyclones, but with several more or less important distinctions and simplifications, about which more is explained in section 2.

We pursue the question raised above in section 3 by starting a numerical experiment with a finite-amplitude vortex (as is usually done) but with a sounding that is neutral to the model cumulus clouds. We find that, for a starting vortex of large enough amplitude, a model-equivalent tropical cyclone can develop in a reasonable time and in the hypothesized manner. We will also investigate in this section the suggestion made in Part I that the geometric size and amplitude of the mature storm may be sensitive to the geometric size of the initial vortex. A final set of sensitivity experiments concerns the steady-state-theory predictions of such important parameters as the maximum tangential wind and surface central pressure drop in terms both of the sea-surface temperature and humidity and of outflow temperature. Since the numerical simulations reach quasi-steady states, we will be in a position to compare the analytic predictions with the numerical results.

In section 4 we examine in detail the model-produced steady-state vortex and evaluate the accuracy of the approximations made in the analytical theory of Part I. As implied by the title of these papers, the air–sea exchange is of paramount importance for the development and maintenance of the hurricane. Serious doubts were raised in Part I concerning the fidelity of boundary-layer representations that do not account for transport of dry midlevel air by either turbulence or precipitating cumuli. In section 4 we diagnose the model's budget of θ_e and find that, beyond a certain distance from the vortex center, the upward transport of θ_e by explicit cumulus convection accounts for most of the flux needed to balance the input at the ocean surface. Section 5 contains our concluding remarks.

2. Description of the model

The governing equations for compressible, axisymmetric flow on an f-plane in the cylindrical coordinates (r, ϕ, z) are

Momentum:

$$\frac{du}{dt}-\left(f+\frac{v}{r}\right)v=-c_p\bar{\theta}_v\frac{\partial\pi}{\partial r}+D_u \tag{1}$$

$$\frac{dv}{dt}+\left(f+\frac{v}{r}\right)u=D_v \tag{2}$$

$$\frac{dw}{dt}=-c_p\bar{\theta}_v\frac{\partial\pi}{\partial z}+D_w+g\left\{\frac{\theta-\bar{\theta}}{\bar{\theta}}+0.61(q_v-\bar{q}_v)-q_l\right\} \tag{3}$$

Conservation of mass:

$$\frac{\partial\pi}{\partial t}+\frac{\bar{c}^2}{c_p\bar{\rho}\bar{\theta}_v{}^2}\left\{\frac{1}{r}\frac{\partial(ru\bar{\rho}\bar{\theta}_v)}{\partial r}+\frac{\partial(w\bar{\rho}\bar{\theta}_v)}{\partial z}\right\}=0 \tag{4}$$

First Law of Thermodynamics:

$$\frac{d\theta}{dt}=M_\theta+D_\theta+R \tag{5}$$

Conservation of water vapor:

$$\frac{dq_v}{dt}=M_{q_v}+D_{q_v} \tag{6}$$

Conservation of liquid water:

$$\frac{dq_l}{dt}=M_{q_l}+D_{q_l}. \tag{7}$$

The seven dependent variables are the velocities in the radial, azimuthal, and vertical directions, (u, v, w); the nondimensional pressure perturbation from the

initial state, π; the potential temperature, θ; the mixing ratio of water vapor, q_v; and the mixing ratio of liquid water, q_l. Quantities with an overbar are initial-state variables which are functions of z only. Remaining symbols are ρ, the density of the air–vapor mixture; c, the speed of sound; c_p, the specific heat at constant pressure of dry air; θ_v, the virtual potential temperature; g, the acceleration due to gravity; f, the Coriolis parameter; and t, the time. The operator d/dt is the substantial derivative,

$$\frac{d}{dt} \equiv \frac{\partial}{\partial t} + u\frac{\partial}{\partial r} + w\frac{\partial}{\partial z}.$$

The symbols M, D and R denote microphysical, diffusive, and radiative processes, respectively, and will be discussed below.

The overall computational strategy for numerically solving (1)–(7) is the same described by KW. The pressure tendency, which would be omitted in the anelastic approximation, is retained in (4); this has the advantage that all dependent variables have prognostic equations which may be simply "marched" forward in time. The computational penalty of having to choose a time step small enough to accommodate the rapidly propagating sound waves is avoided by computing only those few terms associated with sound waves with a small time step, while the rest are advanced with the larger time step appropriate for advective and diffusive processes. For further details the reader is referred to KW.

In seeking the simplest model which retains the essential physics, we have chosen somewhat simpler representations of microphysical and turbulent processes than used in KW or in Willoughby et al.'s version of the KW model; the numerical model described here is similar to that constructed by Willoughby et al. except for certain differences in the microphysics and turbulence representations, the employment in our case of a radiation boundary condition at the outer wall, and our incorporation of a crude representation of radiative cooling. These we describe next.

a. Microphysics

The effects of phase changes of water substance are represented by

$$M_\theta = -\frac{L}{c_p\pi}\frac{dq_{vs}}{dt} \tag{8}$$

$$M_{q_v} = \frac{dq_{vs}}{dt} \tag{9}$$

$$M_{q_l} = -\frac{dq_{vs}}{dt} + \frac{1}{\bar{\rho}}\frac{\partial(\bar{\rho}Vq_l)}{\partial z}, \tag{10}$$

where L is the latent heat of vaporization. The rate of condensation/evaporation is denoted by dq_{vs}/dt. In the present study we consider only one class of liquid water; the only distinction between cloud water and rain water is made in the determination of the terminal velocity of liquid water, V. For $q_l \leq 1$ g kg^{-1}, $V = 0$, while for $q_l > 1$ g kg^{-1}, $V = 7$ m s^{-1}. This procedure (similar to the one used by Takeda, 1966) has the advantage of having to carry one less prognostic equation and is the simplest one which would allow updrafts to unload condensate which, in turn, could fall into unsaturated air to produce downdrafts. A disadvantage of this formulation is that evaporation of falling rain must proceed at a rate sufficient to keep the air saturated, thus the rate of evaporation of rain is greatly exaggerated. The condensation/evaporation technique is applied as follows: if, after an advance over a time step, q_v exceeds q_{vs}, the condensation (and heating) is calculated according to the method of Soong and Ogura (1972) so that the excess is eliminated. If q_v is less than q_{vs}, but q_l is not zero, evaporation takes place and heat is subtracted until either saturation occurs or the liquid water is exhausted, whichever occurs first.

As we will have reason to invoke the conservation of θ_e, we should reiterate (see KW, p. 1073) here that θ_e is not precisely conserved; multiplying (6) by $L/c_p\pi$, adding the result to (5) and using (8) and (9), gives,

$$\frac{d\theta}{dt} + \frac{L}{c_p\pi}\frac{dq_v}{dt} = D_\theta + \frac{L}{c_p\pi}D_{q_v} + R. \tag{11}$$

The standard derivation for the equation for θ_e (e.g., see Dutton, 1976, p. 275–276) replaces $L/c_p\pi$ by $L\theta/c_pT$, where T is the temperature, and then neglects the variation of T so that, in the absence of irreversible processes, an exact differential can be formed, *viz.*

$$\frac{d\theta_e}{dt} \equiv \frac{d[\theta \exp(Lq_v/c_pT)]}{dt} = 0. \tag{12}$$

For purposes of analyses, we will use the conventional definition of θ_e implied by (12), but note that neither the model nor the atmosphere should exactly conserve θ_e, thus defined, even in the absence of irreversible processes.

b. Turbulence

The following development closely parallels that of Mason and Sykes (1982, hereinafter MS) in their two-dimensional numerical simulation of roll vortices. As in a slab-symmetric two-dimensional model, the assumption of axisymmetry allows no direct calculation of turbulent motion, to the extent that real turbulence is three-dimensional. In KW's three-dimensional cloud model, for example, grid-scale motions may be thought of as three-dimensional turbulent eddies, and an energy cascade may be directly computed. When the eddies become too small for the grid, a representation of their effect on the grid-scale motion is required (i.e., a "subgrid parameterization"). In an axisymmetric (or two-dimensional) model *all* turbulent motion is parameterized; that is to say, higher resolution in a model

so constrained does not tell one any more about turbulent motions—it only gives more detail to those features of the simulated phenomena that are axisymmetric. The representation of the turbulence is given by the following:

$$D_u = \frac{1}{r}\frac{\partial r\tau_{rr}}{\partial r} + \frac{\partial \tau_{rz}}{\partial z} - \frac{\tau_{\phi\phi}}{r} \tag{13}$$

$$D_v = \frac{1}{r^2}\frac{\partial r^2\tau_{r\phi}}{\partial r} + \frac{\partial \tau_{z\phi}}{\partial z} \tag{14}$$

$$D_w = \frac{1}{r}\frac{\partial r\tau_{rz}}{\partial r} + \frac{\partial \tau_{zz}}{\partial z} \tag{15}$$

$$D_\theta = -\frac{1}{r}\frac{\partial rF_r^\theta}{\partial r} - \frac{\partial F_z^\theta}{\partial z} \tag{16}$$

$$D_{q_v} = -\frac{1}{r}\frac{\partial rF_r^{q_v}}{\partial r} - \frac{\partial F_z^{q_v}}{\partial z} \tag{17}$$

$$D_{q_l} = -\frac{1}{r}\frac{\partial rF_r^{q_l}}{\partial r} - \frac{\partial F_z^{q_l}}{\partial z}, \tag{18}$$

where the τ are the stresses and the F, the fluxes for the quantities and in the directions designated by the superscripts and subscripts in the conventional way (e.g., see Bird et al., 1960, p. 739).

One can formally derive these equations by beginning with the full governing equations in cylindrical coordinates, azimuthally averaging, and dividing the dependent variable, u, say, into an average, $\overline{u}^\phi$ plus a departure, u' where $\overline{u'}^\phi = 0$. Thus, the above stresses and fluxes may be thought of as the Reynold's stresses and fluxes (e.g., $F_z^\theta \equiv \overline{w'\theta'}^\phi$) due to the azimuthal variations on the azimuthally averaged flow. We relate these stresses and fluxes to the averaged flow in the usual way by the eddy-viscosity assumption;

$$\tau_{rr} = 2\nu\frac{\partial u}{\partial r}, \quad \tau_{\phi\phi} = 2\nu\left(\frac{u}{r}\right), \quad \tau_{zz} = 2\nu\frac{\partial w}{\partial z}$$

$$\tau_{r\phi} = \nu r\frac{\partial}{\partial r}\left(\frac{v}{r}\right), \quad \tau_{rz} = \nu\left(\frac{\partial u}{\partial z} + \frac{\partial w}{\partial r}\right), \quad \tau_{z\phi} = \nu\frac{\partial v}{\partial z},$$

$$F_r^\chi = -\nu\frac{\partial \chi}{\partial r}, \quad F_z^\chi = -\nu\frac{\partial \chi}{\partial z}$$

where here and subsequently χ may denote either θ, q_v or q_l and ν is the eddy viscosity. (For lack of any compelling evidence to the contrary we also use ν for the eddy heat conductivity.) The dependent variables in these and all previous equations should be interpreted as azimuthal averages. Following the Smagorinsky (1963) formulation for ν, we take

$$\nu = l^2 S, \tag{19}$$

where S is the deformation given by

$$S^2 = 2\left[\left(\frac{\partial u}{\partial r}\right)^2 + \left(\frac{u}{r}\right)^2 + \left(\frac{\partial w}{\partial z}\right)^2\right] + \left(\frac{\partial u}{\partial z} + \frac{\partial w}{\partial r}\right)^2 + \left(\frac{\partial v}{\partial r} - \frac{v}{r}\right)^2 + \left(\frac{\partial v}{\partial z}\right)^2 \tag{20}$$

and l is a prescribed mixing length which should be related to some characteristic length of the turbulence and may vary according to local stability properties. To obtain that variation we follow Lilly (1962) and form the energy equation for the turbulence. Assuming equilibrium conditions, one may show

$$-\nu S^2 + F_z^b = -\epsilon, \tag{21}$$

where ϵ is the dissipation. The quantity F_z^b is the vertical flux of buoyancy, the form of which depends on whether or not the air is saturated. If the air is unsaturated,

$$F_z^b = -\nu\frac{g}{\bar{\theta}_v}\frac{\partial \theta_v}{\partial z} \tag{22}$$

and, if saturated,

$$F_z^b = -\nu\left\{A\frac{\partial \theta_e}{\partial z} - g\frac{\partial q_t}{\partial z}\right\}, \tag{23}$$

where

$$q_t \equiv q_v + q_l \tag{24}$$

is the mixing ratio of the total amount of water substance, and

$$A \equiv \frac{g}{\bar{\theta}}\left[\frac{1 + Lq_v/R_dT}{1 + 0.622L^2q_v/c_pR_dT^2}\right], \tag{25}$$

where (23) and (25) are derived by KW. As discussed by KW (p. 1075), θ_e and q_t are *nearly* conserved quantities, and the above mixing scheme is equivalent to a flux-gradient closure on these quantities directly.

On dimensional grounds $\epsilon = \nu^3/l_0^4$, where l_0 is a physical scale typical of the most energetic eddies; substituting this and either (22) or (23) into (21) yields an expression for ν,

$$\nu = l_0^2(1 - \mathrm{Ri})^{1/2}S, \tag{26}$$

where Ri is the Richardson number, defined here as

$$\mathrm{Ri} \equiv \frac{g}{\bar{\theta}_v}\frac{\partial \theta_v}{\partial z}S^{-2} \tag{27}$$

if the air is unsaturated, and

$$\mathrm{Ri} \equiv \left(A\frac{\partial \theta_e}{\partial z} - g\frac{\partial q_t}{\partial z}\right)S^{-2} \tag{28}$$

otherwise. Thus l, introduced in (19), is given by (26). Of course, if Ri > 1, then $\nu = 0$.

As discussed by MS, having a much larger horizontal than vertical grid size (as we will have here) tends to greatly underestimate stresses like τ_{rr} as compared with τ_{rz}. Such an anisotropy could be handled in a second-

order closure model, but in keeping with the general level of complexity of the present model we follow MS and define a horizontal viscosity ν_H based on a horizontal scale of the eddies, l_H. Repeating the procedure used to arrive at (21) for only the horizontal motion gives

$$\nu_H = l_H^2\left\{2\left(\frac{\partial u}{\partial r}\right)^2 + 2\left(\frac{u}{r}\right)^2 + \left(\frac{\partial v}{\partial r} - \frac{v}{r}\right)^2\right\}^{1/2}, \quad (29)$$

which we use in the calculation of τ_{rr}, $\tau_{r\phi}$, $\tau_{\phi\phi}$ and F_r^x. However, in the event that ν as calculated by (26) is greater than ν_H, we use ν in all the stress and flux calculations so that the mixing is isotropic in those regions of strong instability. Values of l_0 and l_H are given, along with other fixed physical parameters used in this study, in Table 1.

c. Radiation

Although we use open lateral boundary conditions (described below), heat is not generally exported from the domain as quickly as it is put in, and, consequently, the mean temperature rises and surface pressure falls over the long integration period (typically ~7 d). The falling surface pressure then artificially increases the saturation equivalent potential temperature at the sea surface and so leads to an artificially large surface heat flux. We attempted to remedy this by prescribing the Newtonian cooling,

$$R \equiv -\frac{(\theta - \bar{\theta})}{\tau_R}. \quad (30)$$

The "radiative cooling" represented by (30) is far from realistic, as it relaxes the temperature profile back toward the initial state rather than toward a state of radiative equilibrium. We therefore consider (30) as representing not so much radiative cooling in a literal sense, but rather as an expedient which allows the environment of the model tropical cyclone to remain similar to the mean hurricane environment, the calculation of which is far beyond the scope of the present model. We take τ_R = 12 h which, as we shall see in section 4, yields cooling rates of approximately 2 K d^{-1} in the outer regions and is approximately enough to balance the gentle but persistent subsidence in the outer regions of the vortex. The cooling rate becomes unrealistically large in the central region where θ becomes significantly larger than $\bar{\theta}$ but, at any given time, is small in comparison to the major terms in the convective region and boundary layer.

We discovered, at a late stage in the present investigation, that the effects of this cooling are more subtle than we had originally believed them to be; in section 3e we describe two experiments, one in which we enforce $|R| < 2$ K d^{-1} and another in which $R = 0$. These experiments show that the Newtonian cooling makes little qualitative difference in the solutions but has a somewhat surprising quantitative effect.

TABLE 1. Model parameters.

Parameter	Value	Equation	Description
l_0	200 m	(26)	Mixing length
l_H	3000 m	(29)	Horizontal mixing length
V	7 m s^{-1}	(10)	Terminal velocity liquid water (=0 if $q_l < 1$ g kg^{-1})
τ_R	12 h	(30)	Time constant, radiative cooling
c^*	30 m s^{-1}	(31)	Wave speed for open boundary condition
z_{sponge}	19.375 km		Bottom of "sponge" layer
α_{max}	0.013 s^{-1}		Maximum value of damping in "sponge" layer
z_{top}	25 km		Domain top
r_{outer}	1500 km		Domain outer radius
Δz	1.25 km		Vertical grid size
Δr	15 km		Horizontal grid size
Δt	20 s		Time step

d. Domain and boundary conditions

In Fig. 1 we show a schematic diagram of the domain and arrangement of the dependent variables, (u, v, w) on the "staggered-grid" (e.g., see Lilly, 1964) spanning the domain. The other dependent variables are all defined at the v point.

On the centerline there is, by the assumption of axisymmetry, no radial flow (u = 0). The only other constraints are the ones associated with diffusion; we set $\tau_{rz} = 0$, $\tau_{r\phi} = 0$, and $F_r^x = 0$ at $r = 0$.

At the upper boundary we place a rigid lid (w = 0) and we set $\tau_{rz} = 0$, $\tau_{z\phi} = 0$, and $F_z^x = 0$ at $z = z_{top}$. To damp out gravity waves before they can reflect from the rigid lid back into the lower troposphere, we employ a "sponge" layer in the uppermost portion of the model domain. The height of the lowermost part of the sponge layer is chosen to be well above the tropopause, so that the convection will be limited in height by physical processes near the tropopause. Thus the sponge layer is simply a "graveyard for old gravity waves" and plays no role in limiting the vertical extent of the circulation. We add the Newtonian damping,

$$-\alpha(z)(\psi - \bar{\psi}),$$

to the right-hand side of all prognostic equations except for the one for π (ψ is any of the dependent variables save π). $\alpha = 0$ for $z \leq z_{sponge}$ then increases to α_{max} at $z = z_{top}$ in the manner described by Durran and Klemp (1983, p. 2345; see Table 1 for parameter values used herein).

Because the numerical integration must be executed on a finite domain, one must seek conditions which let the fluid behave as if there were no outer limit at $r = r_{outer}$. In the present study r_{outer} = 1500 km and, as

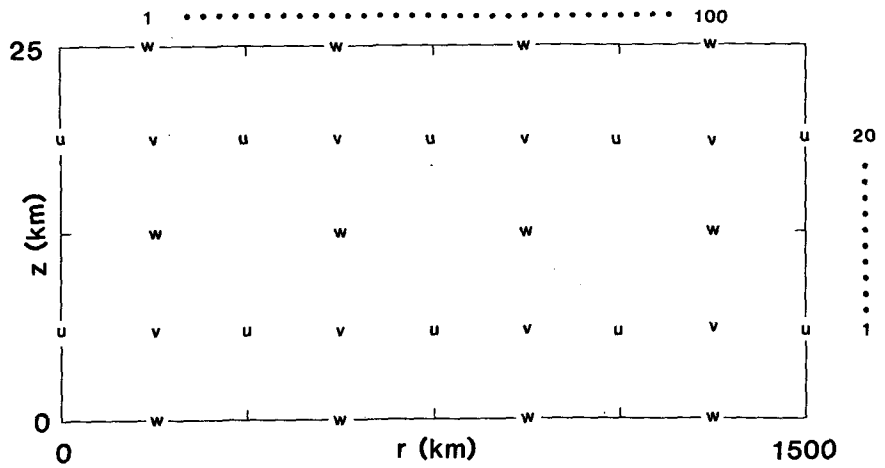

FIG. 1. Domain and arrangement of dependent variables on the staggered grid covering the domain. All "thermodynamic" variables are located at the v points.

we shall see in section 4, the computed transverse circulation extends to approximately 1000 km and so is well within r_{outer}. The implied subsidence in the return flow leads to heating which is balanced by the radiational cooling discussed above. Thus, a rigid wall (i.e., $u = 0$) at $r = r_{\text{outer}}$ might at first seem sufficient. However, cumulus convection, in the outer regions of the vortex, produces internal gravity waves; to allow these waves to exit radially at $r = r_{\text{outer}}$, we follow KW (p. 1077) and replace (1) at $r = r_{\text{outer}}$ with

$$\frac{\partial u}{\partial t} + (u + c^*)\frac{\partial u}{\partial r} = \left(f + \frac{v}{r}\right)v, \tag{31}$$

where c^* is an approximated intrinsic phase velocity of the dominant gravity wave modes moving out through the boundary. The horizontal advections for all other dependent variables (save π) are calculated by one-sided differences [if $u > 0$, otherwise they are set to zero; likewise if, in (31) $u + c^* < 0$, then this term is set to zero]. The radial stresses and fluxes are chosen so that the first terms on the right-hand sides of (13)–(18) vanish at $r = r_{\text{outer}}$. See KW and the study by Hack and Schubert (1984) for further details.

At the lower surface we require that the normal velocity vanish ($w = 0$). The tangential stresses and vertical fluxes at the surface are given by the bulk aerodynamic formulas:

$$\tau_{rz} = [C_D u(u^2 + v^2)^{1/2}]_{\Delta z/2} \tag{32}$$

$$\tau_{z\phi} = [C_D v(u^2 + v^2)^{1/2}]_{\Delta z/2} \tag{33}$$

$$F_z^{\theta} = [C_E(u^2 + v^2)^{1/2}]_{\Delta z/2}(\theta_{\text{surf}} - \theta|_{\Delta z/2}) \tag{34}$$

$$F_z^{q_v} = \{C_E\sqrt{u^2 + v^2}\}_{\Delta z/2}(q_{v\,\text{surf}} - q_v|_{\Delta z/2}). \tag{35}$$

We set $F_z^{q_l} = 0$ at $z = 0$, but water may leave the domain by falling through the lower boundary. The C_D and C_E are the drag coefficients for momentum and heat (sensible and latent), respectively, which, unless otherwise mentioned, are taken to be equal and given by Deacon's formula,

$$C_D = 1.1 \times 10^{-3} + 4 \times 10^{-5}(u^2 + v^2)^{1/2}|_{\Delta z/2} \tag{36}$$

(e.g., see Moss and Rosenthal, 1975). We decided to use this admittedly complicated form after having experimented with a constant C_D. With constant $C_D = 1.1 \times 10^{-3}$, we found the transfer rate of moist entropy from the sea surface too small to obtain a tropical cyclone in a reasonable time; letting $C_D = 3.0 \times 10^{-3}$ allows for a reasonable development time but is much too large for the outer sections of the vortex, where the wind is much weaker, and distorts the budget of moist entropy in the boundary layer.

Also, at $z = 0$, we specify the temperature, $T = T_{\text{surf}}$, as constant (see Table 2); because $\theta_{\text{surf}} = T_{\text{surf}}/\pi_{\text{surf}}$ and we set $q_{v\,\text{surf}} = q_{vs}(T_{\text{surf}}, \pi_{\text{surf}})$, both θ_{surf} and $q_{v\,\text{surf}}$ are functions of the dependent variable π and so will vary through the calculation. This dependence then allows for heat and moisture addition due to isothermal expansion.

The procedure for obtaining a numerical solution of the finite-difference analogues to the model equations, where it departs from that of KW, is given in the Appendix. The reader wishing to skip this should be aware of the following few basic pieces of information about the numerical model. We take $r_{\text{outer}} = 1500$ km and $z_{\text{top}} = 25$ km and cover this domain by 100 and 20 grid distances in the horizontal and vertical, respectively, so that the radial grid size $\Delta r = 15$ km, and the vertical grid size $\Delta z = 1.25$ km. The "sponge" layer begins at 19.375 km (grid level number 16 for the v point). The large time step $\Delta t = 20$ s, so that a total of 32 400 time steps are required to integrate out to 180 h, the time by which the solutions become nearly steady. The initial conditions used in this study are somewhat novel and will be described in the following section.

TABLE 2. Numerical experiments.

Exp	Initial vortex v_{max} (m s^{-1})	Initial vortex r_m (km)	Initial vortex r_0 (km)	T_{surf} (°C)	Tropopause (mb)	Comments
A	12	82.5	412.5	26.3	100	Control run
B	2	82.5	412.5	26.3	100	Weak vortex
C	12	160.0	800.0	26.3	100	Large vortex
D	12	41.0	206.0	26.3	100	Small vortex Δr = 7.5 km, r_{outer} = 750 km, l_H = 1500 m
E	12	82.5	412.5	26.3	100	Dry to 30% RH above boundary layer
F	12	82.5	412.5	26.3	300	Increase tropopause
G	12	82.5	412.5	31.3	100	Increase SST
H	12	82.5	412.5	31.3	200	Increase SST and lower tropopause
I	12	82.5	412.5	31.3	300	Increase SST and lower tropopause
J	12	82.5	412.5	26.3	100	Limited Newtonian cooling $\|R\| < 2$ K d^{-1}
K	12	82.5	412.5	26.3	100	Zero Newtonian cooling $R = 0$

3. Evolution from a "model-neutral" state

Our philosophy in creating the initial thermodynamic state of the model is central to the objectives of this investigation. We hold that the average state of the tropical atmosphere in summer, as represented, say, by Jordan's (1958) sounding, is very nearly neutral to *real* convection, which is observed to be, on average, highly dilute. If this were not so, strong convection would erupt spontaneously and would drive the atmosphere toward neutrality. Our view is thus closely related to the quasi-equilibrium supposition of Arakawa and Shubert (1974). In accord with this view, it is important to recognize that while Jordan's sounding may be nearly neutral to actual clouds, the numerical model's version of "clouds" may (and usually does) grow rapidly in the same environment. We see this artificial conditional instability as a major hindrance to a clear interpretation of the initial development of tropical cyclones in numerical simulations performed to date. Within the confines of an axisymmetric model, the artificially intense clouds invariably lead to an upscale transfer of energy (similar in concept to Fjortoft, 1953), which may well result in a cyclone-scale rotating thunderstorm, as happens, for example, in the simulation by Yamasaki (1977), which relies entirely on a maintained large reservoir of convective available potential energy, and which produces a small-scale vortex that reaches maturity in about 40 hours. We therefore create an initial condition that is neutral to the model's convective clouds. Our construction of this "model-neutral" initial state may be viewed as an attempt to create a similarity between the relationship of actual cumulus clouds to the real atmosphere and the relationship of model clouds to the model atmosphere.

The model-neutral state is created as follows: we take a model domain with a wall placed at r_{outer} = 450 km, set v and $f = 0$, and prescribe for u and w forms which represent several convergence zones; no heat or moisture is added ($\theta = \bar{\theta}$, $q_v = \bar{q}_v$, and $q_l = 0$) and surface fluxes and radiative cooling are not allowed. Convection occurs and, after several hours, extinguishes the instability. The modified sounding is shown in Fig. 2; the stabilization is manifested by a drying of the lower layers and a slight warming of the middle layers.

a. Control experiment

We begin the simulation by specifying the vortex tangential velocity

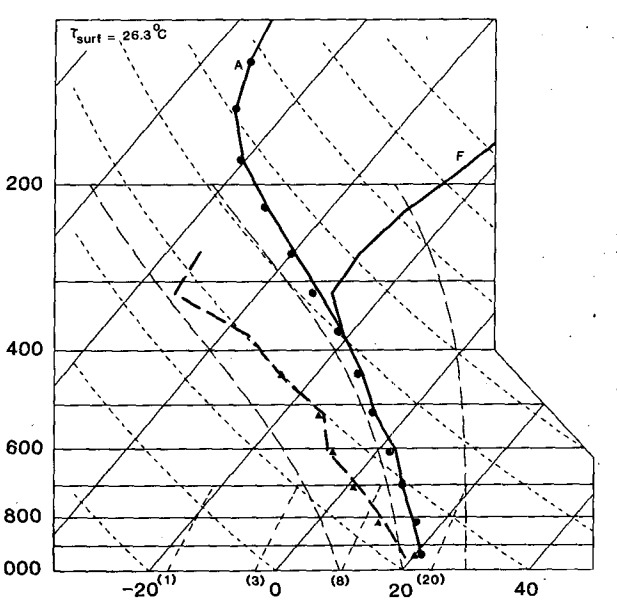

FIG. 2. Jordan's (1958) sounding interpolated to the model grid levels is indicated by the dots and triangles. The curve labeled "A" is the Jordan sounding mixed to conditional neutrality (Exp. A). The effect of having a warmer outflow is investigated in Exp. F where the tropopause is lowered to 300 mb. Here and subsequently we label the dry adiabats and the isotherms at their intersection at p = 1000 mb. Mixing ratio lines are labeled in parentheses. Three moist adiabats are also indicated as long-dashed lines.

$$v(r,z,0)=\frac{z_{\text{sponge}}-z}{z_{\text{sponge}}}\left\langle\left\{v_m{}^2\left(\frac{r}{r_m}\right)^2\left[\left(\frac{2r_m}{r+r_m}\right)^3-\left(\frac{2r_m}{r_0+r_m}\right)^3\right]+\frac{f^2r^2}{4}\right\}^{1/2}-\frac{fr}{2}\right\rangle \quad (37)$$

where r_0 is the outer radius of the vortex beyond which $v = 0$. The quantities v_m and r_m are approximately the maximum wind and radius of maximum wind, respectively (they become exactly so in the limit of large r_0/r_m and v_m/fr_m). We arbitrarily let the intensity decay linearly with height, so that $v = 0$ at $z = z_{\text{sponge}}$, and we let $v = 0$ for $z > z_{\text{sponge}}$. The temperature field is adjusted so that the vortex is in thermal wind balance. For the control experiment (which we designate as Exp. A), we choose $r_0 = 412.5$ km, $r_m = 82.5$ km, and $v_m = 15$ m s^{-1} (giving $v_{\max} \approx 12$ m s^{-1}); this leads to a temperature adjustment of at most $\sim$0.6 K at the vortex center. The sea-surface temperature, $T_{\text{surf}} = 26.3$°C (see Table 2).

In Part I it is conjectured that the hurricane develops purely through an air–sea interaction instability. Figure 3 contains a time series of $v_{\max}$ and shows that in the control experiment a hurricane-intensity vortex may develop from a state which is neutral to the model's convection. We show in Fig. 4 that $\theta'_e \equiv (\theta_e - \bar{\theta}_e)$ with v superimposed to illustrate the manner in which the model hurricane develops. As the vortex winds pass over the ocean surface, θ_e is transferred to the interior as prescribed by (34)–(35) and leads locally to conditional instability, cumulus convection, and subsequently precipitation. As cool, dry, midlevel air descends to the surface, convective activity slows until more moist entropy can by transferred into the atmosphere from the surface to fuel further convection. Eventually, the middle atmosphere in this region is moistened to the extent that downdrafts can no longer keep the boundary layer cool. The vortex winds gradually intensify, the sea-surface transfer of θ_e is enhanced near the region of strongest wind and low pressure, and a steadily amplifying circulation develops after 80 h or so.

It is difficult to find any conditional instability (as measured by the positive area on a tephigram) at any of the times shown in Fig. 4. This is because as instability develops it is almost immediately quenched by convection. Considering that Fig. 4 contains only three time steps out of a possible 32 400, one would have to look very carefully for times and locations at which conditional instability exists. This is simply another

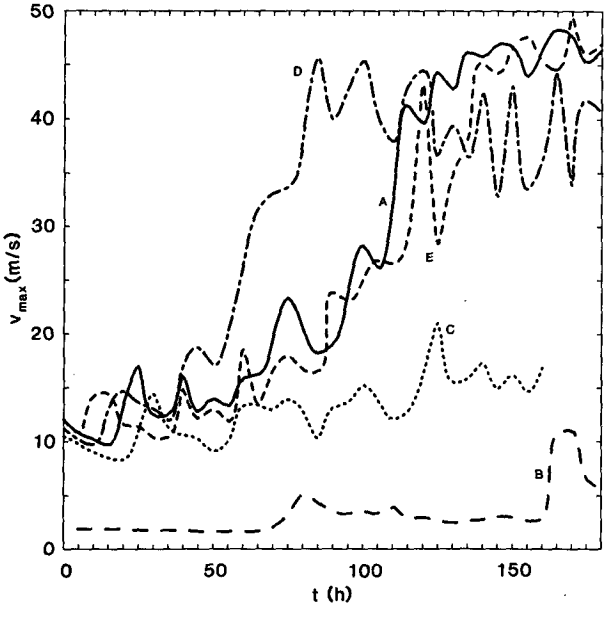

FIG. 3. Time series of $v_{\max}$ for Exps. A–E (defined in Table 2).

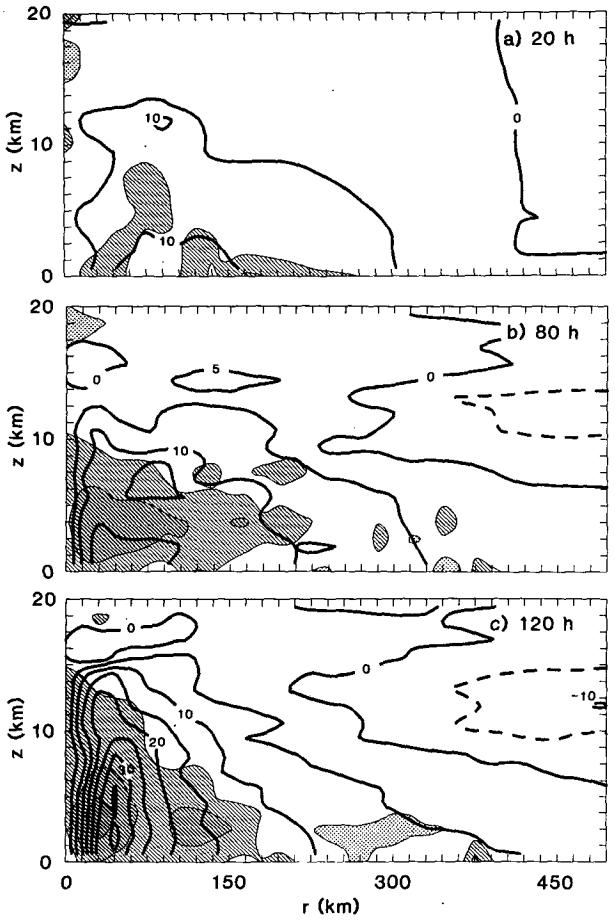

FIG. 4. θ'_e, the deviation of θ_e from its initial value, $\bar{\theta}_e$ shaded in increments of 5 K; the lightest shading indicates $5 < \theta'_e < 10$ K, the darker shading indicates $10 < \theta'_e < 15$ K, and the darkest shading indicates $\theta'_e > 15$ K; the stippled region shows where $\theta'_e < -5$ K. The azimuthal velocity is superimposed and represented by contour lines in intervals of 5 m s^{-1} at (a) $t = 20$, (b) $t = 80$ and (c) $t = 120$ h. Here and subsequently we display the model data on a 495 × 20 km portion of the domain (33 × 16 grid levels) for clarity of presentation.

way of saying that the model cumulus clouds are simply agents which transfer heat from the oceanic source to the upper atmospheric sink on a time scale far shorter than that of the evolving vortex.

The absence of conditional instability is broadly consistent with the findings of previous modeling efforts even though these used unstable initial conditions. In an experiment by Willoughby et al. (1984, Fig. 12), for example, the initial conditional instability was exhausted by about 20 hours after the initialization, and at least 10 hours before the large-scale vortex started to amplify. The evolution and structure in their model is quite similar to the results described here.

We will examine the steady-state structure in more detail in section 4, but, before moving on to the sensitivity experiments, we display in Fig. 5 $u, v, w, p' \equiv (p - \bar{p})$, $T' \equiv (T - \bar{T})$, q_v and q_l fields averaged over 20 hours (160–180 h, when the solution is nearly steady) to show that the solutions are broadly similar to those obtained in previous modeling studies (e.g., see Kurihara and Tuleya, 1974; or Rosenthal, 1978). The azimuthal wind field is characterized by a sharp maximum at low-levels at ~40 km and anticyclonic flow at upper levels and outward from the center; the pressure-perturbation field exhibits a sharp drop within the inner ~75 km and decays with height; the field of radial motion shows strong inflow in the boundary layer, outflow aloft, and a minor inflow at middle levels; the vertical velocity maximizes off the central axis and forms the "wall" surrounding the "eye" where, both

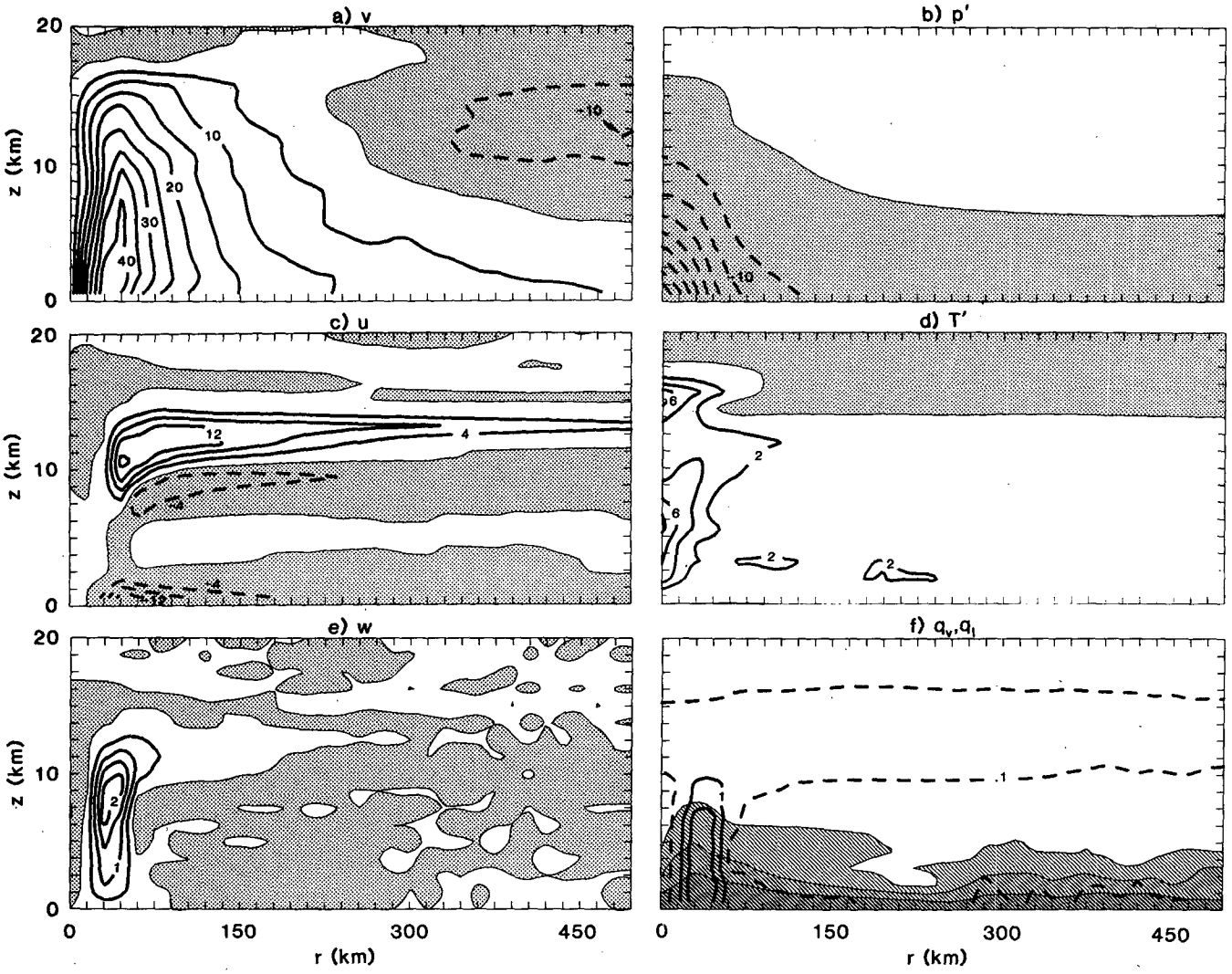

FIG. 5. The 160–180 h average fields for the nearly steady state reached in the control run. All stippled regions indicate negative values of the field (a) Azimuthal velocity, contour interval, 5 m s^{-1}; (b) dimensional pressure deviation from the initial state, contour interval, 5 mb; (c) radial velocity contour interval, 4 m s^{-1}; (d) temperature deviation from the initial state, contour interval, 2 K; (e) vertical velocity, contour interval, 0.5 m s^{-1}; (f) liquid water, contour interval, 1 g kg^{-1}; dashed line denotes the 0.1 g kg^{-1} contour, and water vapor; lightest shading indicates $3 < q_v < 8$ g kg^{-1}, [illegible] shading indicates $8 < q_v < 13$ g kg^{-1}, and darkest shading indicates $q_v > 13$ g kg^{-1}.

there and outside of the "eyewall", subsidence occurs; the perturbation-temperature field exhibits a warm core with subsidence warming extending outward at the top of the boundary layer and aloft; the q_v field also shows the effect of strong subsidence near $r \sim 210$–240 km, while inside this radius the air approaches saturation as $r \to 0$ and outside this radius the distribution, although disturbed, is close to the initial distribution of q_v; the q_l field forms the outline of a shank of cloud in the eyewall with an anvil extending outward aloft and with several smaller patches of saturated air beyond the radius of intense subsidence; the most intense concentrations of q_l represent rain in the eyewall. The eddy viscosity (not shown) is, generally speaking, nonzero only in saturated regions where $\nu_{\max} \approx 10^2$ m^2 s^{-1}. The horizontal eddy viscosity, ν_H is appreciable where v is largest and obtains maximum values $\approx 10^4$ m^2 s^{-1}.

In order to test the effect of model resolution and domain size on the solutions, we performed a number of experiments in which we respectively doubled the vertical resolution, decreased the horizontal grid size to 10 km, and removed r_{outer} to 2010 km; in each case all the other model parameters were identical to those used in the control run. We observed very little variation from the basic features shown in Fig. 5.

b. *Sensitivity to the initial vortex*

In Part I it was suggested that tropical cyclone development might be a consequence of a *finite-amplitude* instability. To test this idea with the current model, we conduct several experiments varying the parameters in (37) (see Table 2).

In Exp. B we set v_m such that the maximum velocity is ~ 2 m s^{-1}. The history of the development is shown in Fig. 3; owing to the low velocity, latent-heat transfer is slow and cumulus convection does not start until ~ 70 h. After this time, there is convection, but the cool, dry, downdrafts extinguish the instability before the vortex can build up enough speed to increase significantly the sea-surface transfer. At some point in the distant future, the vortex may ultimately amplify, but for all practical purposes we may conclude that the weaker-amplitude vortex does not grow.

It was also suggested in Part I that if the initial vortex covers too large an area amplification would be difficult. In Exp. C, r_m and r_0 are approximately doubled (see Table 2). Figure 3 summarizes the ensuing development. Over the entire period the vortex intensifies only a slight amount. Analysis of the model data reveals that with such a large vortex, convection is spread over such a broad area that the central region does not become moist enough to prevent cool downdrafts from keeping θ_e low in the boundary layer.

It has long been known that the existence of an upper-level anticyclone is a precursor to hurricane formation (Riehl, 1954, p. 332). To test whether such an initial vortex might lead to a more rapid development within the confines of the present model, we needed some method to obtain a reasonable first guess for such a vortex. We settled on the following: since setting $C_E = 0$ causes the demise of the model hurricane (Ooyama, 1969), we can arrive at a vortex of surface intensity comparable to the one used to initiate the control run by setting $C_E = 0$ at $t = 180$ h, and then integrating forward until $v_{\max}$ drops off to ~ 12 m s^{-1}. The upper anticyclone does not decay so rapidly and so we have the desired initial vortex. Aside from adjusting the potential temperature for thermal-wind balance, we set $q_v = \bar{q}_v$, $\theta = \bar{\theta}$, and $q_l = 0$ so that the initial thermodynamic state is essentially the same as for the control run (Fig. 2). The ensuing development was nearly identical to the control run indicating the insensitivity of the model vortex development to the initial upper anticyclone.

One final experiment along these lines was conducted to test the conjecture made in Part I that the horizontal size of the mature vortex depends on the horizontal size of the initial vortex up to a certain large-scale limit, which depends on the length scale $(c_p T_B)^{1/2} f^{-1}$. To do this we tried to "fool" the vortex by cutting all horizontal lengths in half: the geometric size (r_m and r_0) of the initial vortex, horizontal grid scale, mixing length, and domain size are all halved (Exp. D; see Table 2). The ensuing development is summarized in Fig. 3: the vortex develops more quickly and reaches only a slightly less intense state than did the control-run vortex and is much less steady. Of course, the vortex cannot be totally "fooled" since the convective motions become more vigorous with the smaller horizontal grid; hence the greater unsteadiness is expected. Notwithstanding, the general structure of the vortex is similar to the control-run vortex, except that it is approximately one-half the horizontal size. This experiment supports the conjecture that, within a large-scale limit, the size of a mature tropical cyclone is determined by the size of the initial disturbance; this is in turn consistent with the observation that tropical cyclones of vastly different scales not only occur, but coexist in the same locale (Merrill, 1984).

c. *Sensitivity to the initial relative humidity*

The corrosive effects of cool, dry downdrafts on the early development of the vortices were much in evidence in the experiment described above. Experiment E is identical to the control experiment except that the initial relative humidity everywhere above the lowest grid level is dropped to 30% (Fig. 2 indicates the relative humidity is generally greater than 50% below 500 mb in the control run). The time history of the experiment (Fig. 3) shows that the steady state is reached approximately 2–3 days later than in the control run. Eventually, the inner region of the vortex moistens to saturation, and the final steady-state vortex is, for all intents and purposes, identical to the control vortex.

d. *Sensitivity to the temperature at sea surface and tropopause*

Perhaps the most important conclusion of Part I is that useful predictions can be made by considering the hurricane to be energetically similar to a simple Carnot engine. Equation (26) of Part I expresses a simple relation between the central pressure drop, sea-surface and outflow temperature, and difference between the ambient and central relative humidity in the boundary layer, and may be derived from the Carnot principle. A simple albeit ad hoc boundary-layer theory was used to close the mathematical problem and thus provide a prediction for v_{max} in terms of the aforementioned parameters. We can test the predictions of that theory here by specifying different sea-surface temperatures and, by changing the height of the tropopause, altering the outflow temperature.

The tropopause in the control run is at approximately 100 mb. The modified Jordan sounding shown in Fig. 2 is further altered by lowering the tropopause to 300 mb and this defines Exp. F. The time-history of v_{max} for this experiment is shown in Fig. 7. Exps. G, H and I are conducted with T_{surf} = 31.3 C and the tropopause at 100, 200 and 300 mb, respectively. Simply specifying an increased T_{surf} with the modified Jordan sounding of Fig. 2 would lead to tremendous conditional instability. To avoid this we let the potential temperature at the first grid level (625 m) equal the sea-surface value and assign q_v at this same level so that the relative humidity near the surface (anemometer level) is approximately 80%. Then, as described previously, an integration is carried out to obtain the *model-neutral* soundings which are displayed in Fig. 6. The time histories for these experiments are shown in Fig. 7.

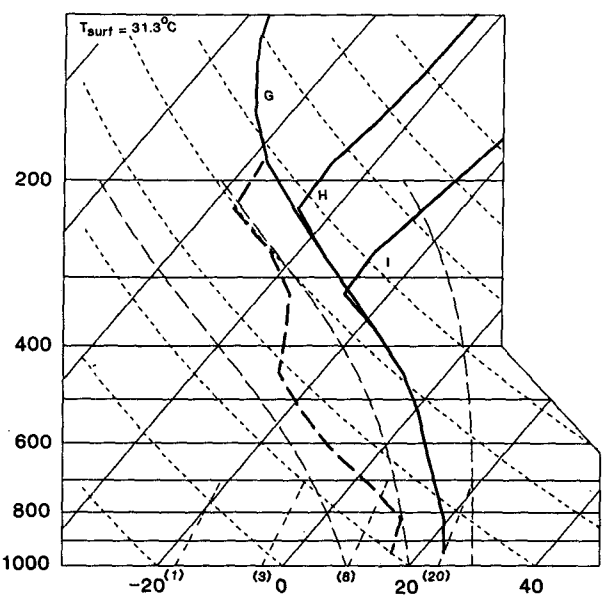

FIG. 6. Model-neutral soundings for T_{surf} = 31.3 C with the tropopause at 100, 200 and 300 mb (Exps. G, H and I, respectively).

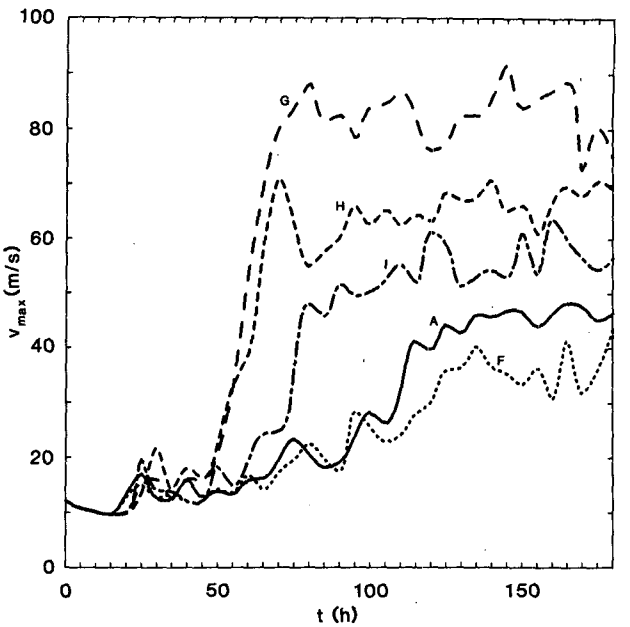

FIG. 7. Time series of v_{max} for Exps. A, F, G, H and I (defined in Table 2).

Table 3 contains a comparison of the theoretically predicted central pressure, p_c and maximum velocity, v_{max} [calculated respectively from (26) and (43) of Part I; we let the relative humidity at the vortex center, RH_{cs} = 100% while the other parameters used in these formulas are given in Table 3] against their numerically obtained counterparts for Exps. A, F, G, H and I. T_B is the temperature at the top of the boundary layer which we take here to be the temperature at $z = \Delta z/2$ from the model data. The RH_{as} is the ambient relative humidity at the surface, which we calculate from the model data by assuming a constant mixing ratio and potential temperature from the first grid level (625 m down to the top of the surface layer) and by observing that outside the zone of intense subsidence the air is nearly saturated at z = 625 m.

The outflow temperature, $\bar{T}_{out}$ is calculated from (19) of Part I, viz.,

$$\bar{T}_{out} = \frac{1}{\ln \dfrac{\theta_e}{\theta_{ea}}} \int_{\ln\theta_{ea}}^{\ln\theta_e} T d(\ln\theta_e),$$

where θ_{ea} is the ambient θ_e. To compute $\bar{T}_{out}$ from the model data, we compute the trajectory of a parcel rising through the eyewall using the 160–180 h averaged patterns for Exps. A, F, G, H and I and record both T and θ_e as a function of the parcel's position. Thus, as the parcel begins its descent at large radius we can, by noting at which position the parcel achieves its original θ_e ($=\theta_{ea}$), calculate the average defined above. (This av-

TABLE 3. Comparison of theory and numerical experiment.

	Numerical experiments*										Theory		
Exp	T_S (°C)	$\bar{T}_{out}$ (K)	$(\bar{T}_{out})^{\dagger}_{est}$ (K)	T_B (K)	ϵ	r_{max} (km)	r_0 (km)	RH_{as} (%)	p_c (mb)	v_{max} (m s^{-1})	p_c (mb)	v_{max} (m s^{-1})	r_0 (km)
A	26.3	228	203	295.	.23	38	400	81.8	973	46	975	48	380
F	26.3	245	244	295.	.17	45	400	81.8	991	38	989	42	340
G	31.3	207	197	298.	.31	30	900	78.6	903	77	903	72	570
H	31.3	227	227	298.5	.24	40	750	78.6	937	66	944	63	490
I	31.3	246	246	298.5	.18	50	700	78.6	964	55	972	54	430
J	26.3	216	203	295.	.27	38	340	81.8	961	51	961	53	440
K	26.3	212	203	295.	.28	38	370	81.8	957	57	956	59	450

* Obtained from average over 160–180 h.
† Estimated using method described in Part I. Not used in predictions of p_c and v_{max}.

erage multiplied by $c_p \ln(\theta_e/\theta_{ea})$ is simply the heat lost at the cold reservoir in the Carnot cycle which we will examine more thoroughly in the next section.) The outflow temperature calculated this way is a function of the fully developed vortex structure; in Part I a way of estimating T_{out} from the initial sounding was suggested. That method relies on the assumption that individual parcels will flow out of the system at their level of neutral buoyancy, calculated from the initial sounding; T_{out} estimated this way is a purely external parameter. Table 3 compares this estimate of T_{out} with the calculated value; except for the control run, agreement is good. We return to this point in the next subsection.

The geometric size of the vortex is difficult to define with precision; we arbitrarily choose the radius where $v = 10$ m s^{-1} as r_0. Fortunately, the formulas (26) and (43) of Part I are not sensitive to the value of r_0 within the range under present consideration. Equation (46) of Part I provides a theoretical prediction for the relationship between r_{max} and r_0 (though not for the absolute value of either). Because r_{max} is less ambiguous than r_0, we compute r_0 given r_{max} and the other parameters and show the result in Table 3.

The agreement between theory and numerical experiment concerning p_c and v_{max} is generally good (within 10%) and in some cases excellent (within 1%). The agreement concerning r_0 is not very good because, we believe, of the aforementioned ambiguity in the determination of r_0 from the model data, and because the radius of maximum winds is poorly resolved by the present model. However, it is encouraging that the variation of the model r_0 follows the variation of the theoretically predicted value. We should add that the theoretical predictions of v_{max} and r_0 depend on a crude boundary layer, while the prediction of p_c is independent of the boundary layer. The good agreement between the predicted and model-produced values of p_c may be understood in terms of the Carnot cycle described in section 3 of Part I. Unlike the derivation of the minimum central pressure given in section 2 of Part I, the Carnot-cycle prediction does not rely on neutrality to slantwise moist convection everywhere in the vortex.

e. *Sensitivity of T_{out}*

That the model-calculated T_{out} is so much different from the estimated value in Exps. A and G can be explained by observing that the soundings in these cases become nearly tangent to the moist adiabats near the tropopause; small changes in a rising parcel's temperature lead to a large change in its outflow level and temperature. In general, the updraft air may be "diluted" through mixing with the environment and so exit at a lower (warmer) level. Another reason the model outflow temperature may be much warmer than the estimated value is that the Newtonian cooling, as represented by (30), produces unrealistically large cooling rates in the inner core. At first glance this seems paradoxical, but the formulation works in much the same way as the "dilution" effect—as a parcel rises through the updraft, (30) requires that it lose buoyancy. Therefore, the parcel exits the updraft at a lower level, and T_{out} is larger than it would have been in the absence of such cooling.

To test this, we conducted two experiments identical to the control run, except in the first we required that $|R| < 2$ K d^{-1} (Exp. J) and, in the second, we let $R = 0$ (Exp. K). The first formulation allows for subsidence warming in the outer region of the vortex to be approximately balanced, but keeps the cooling in the inner part of the vortex to within a physically reasonable bound; the second formulation allows the entire domain to warm over time. Table 3 shows that in Exps. J and K, $T_{out} \approx 216$ and 212 K, respectively; thus restriction or removal of the Newtonian cooling produces a colder outflow (and a more intense vortex). Figures 8a, b show the T' fields for Exps. J and K (compare with Fig. 5d); with less cooling, these plots show larger temperature perturbations higher up which more nearly resemble observations (e.g., see Hawkins and Imbembo, 1976). The other fields are qualitatively similar to the control run and differ quantitatively as

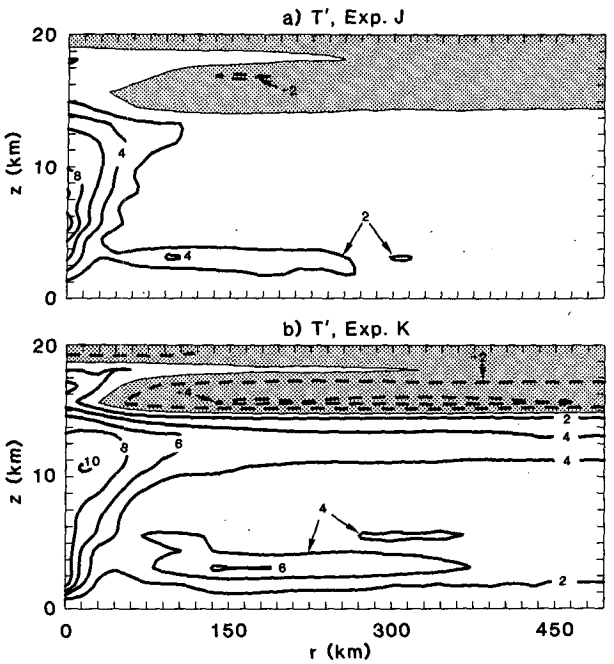

FIG. 8. Perturbation temperature, T', as in Fig. 5d for (a) Exp. J and (b) Exp. K. See Table 2.

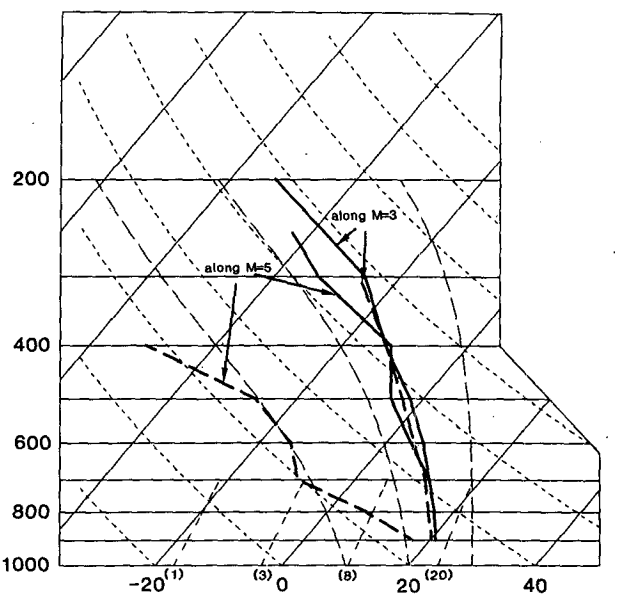

FIG. 10. Soundings along the $M = 3$ and $M = 5$ surfaces shown in Fig. 9.

indicated in Table 3. Again, using the model-calculated T_{out} in the analytical formulas of Part I gave very good agreement between model and theory for p_c and v_{max}.

In summary, our use of (30) unexpectedly led us to discover a strong model sensitivity to the shape of the tropopause; Exps. F, H and I have a "sharp" tropopause which allows the model-produced T_{out} to be almost exactly the theoretical value, despite the unrealistically large cooling. In these cases, the estimate of T_{out} provides an excellent prediction of the final model-produced p_c and v_{max}. In Exps. A and G, the unrealistic Newtonian cooling has a much larger effect on the outflow temperature owing to the structure of the tropopause. However, not all of the discrepancy between the estimated and model-calculated T_{out} can be attributed to the Newtonian cooling because, even in the case where $R = 0$, the model-calculated outflow temperature is still 9 K warmer than the estimated value. Our analysis of the θ_e budget of the control run shows that radial mixing ("dilution") produces cooling rates of approximately -1 to -1.5 K h^{-1} in the eyewall. Since it takes a parcel approximately 2 h to rise through the updraft, its θ_e may decrease by approximately 2–3 K. Thus, a parcel starting its ascent on one moist adiabat may find itself on another, 3 K-cooler, moist adiabat by the time it reaches the tropopause—this can easily account for the 9 K warmer outflow temperature given the shape of the tropopause in the control run.

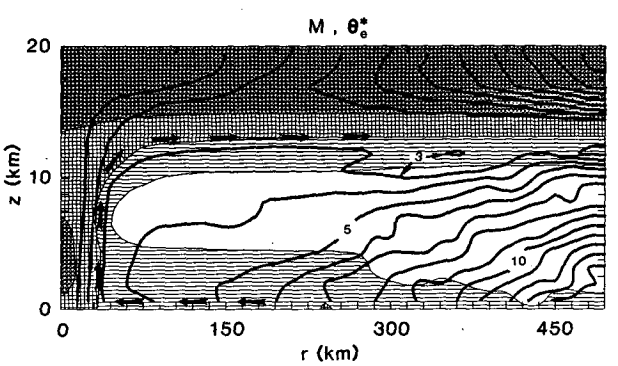

FIG. 9. θ_e^* and M surfaces for the control run at averaged over 160–180 h when the solution is nearly steady. The areas shaded by horizontal lines indicate $345 < \theta_e^* < 350$ K, the areas shaded by horizontal and vertical lines indicate $350 < \theta_e^* < 360$ K, and the darkest shading indicates where $\theta_e^* > 360$ K. The angular momentum surfaces are labeled in nondimensional units ($M[r = r_{outer}] = 100$). Also shown is a streamline through the updraft.

4. Steady-state structure

a. *Conditional neutrality along angular-momentum surfaces*

A central hypothesis of the analysis in Part I is that slantwise moist convection establishes a one-to-one relation between saturated moist entropy, θ_e^* and angular momentum, $M \equiv rv + fr^2/2$. Figure 9 shows θ_e^* and M with a streamline through the updraft (in the r–z plane) superimposed for Exp. A.[1] In the region of the basic circulation in the r–z plane, θ_e^* and M surfaces

[1] It should be recalled that θ_e defined by (12) is not exactly conserved by the model. Maximum departures from the model-conserved quantity are estimated to be a few degrees centigrade.

are congruent as hypothesized. To further illustrate this point Fig. 10 contains soundings along the $M = 3$ and $M = 5$ surfaces shown in Fig. 9. On the $M = 3$ surface rising up within the eye wall, Fig. 10 shows there is almost perfect conditional neutrality for all parcels along the path. The M surface rising out of the boundary layer beneath the ring of subsidence also exhibits conditional neutrality to displacements of the nearly saturated boundary-layer air; however, owing to the extreme dryness of the middle atmosphere, displacements of all other parcels are conditionally stable.

The question naturally arises, "How did the initially orthogonal surfaces of θ_e^* and M become congruent?" Figure 11 shows the θ_e^* and M surfaces in the developing vortex at $t = 20$, 80 and 120 h. In lower portions of the atmosphere, high-θ_e air created at the surface is transported upward, and, thus, lines of constant θ_e^* become parallel to the nearly vertical lines of constant M. As noted in all previous modeling studies, the configuration in the upper outflow region tends to be locally unstable to symmetric disturbances (e.g., see Kurihara, 1975, Fig. 33). Figure 11 illustrates how convective updrafts give rise to local maxima of M and thereby render the flow symmetrically unstable (see also Willoughby et al., 1984, p. 1181). After some vigorous mixing, a compromise between the initially horizontal θ_e^* and the initially vertical M surfaces is found, resulting in both surfaces inclining to the horizontal and thus appearing to "flare" out in the final steady state. We note that the congruity of M and θ_e^* surfaces must be achieved by irreversible processes, since the angle between them is proportional to the moist potential vorticity, which is conserved.

To the extent that the vortex is neutral to slantwise moist convection, the vertical circulation has no feedback on the balanced part of the flow and may be considered to be mechanically forced by surface friction acting on the balanced flow. Examination of Fig. 5 shows that the sign of the vertical velocity near the lower boundary is consistent with the predictions of Ekman theory, with rising motion in regions of positive relative vorticity and descent where the relative vorticity is negative.

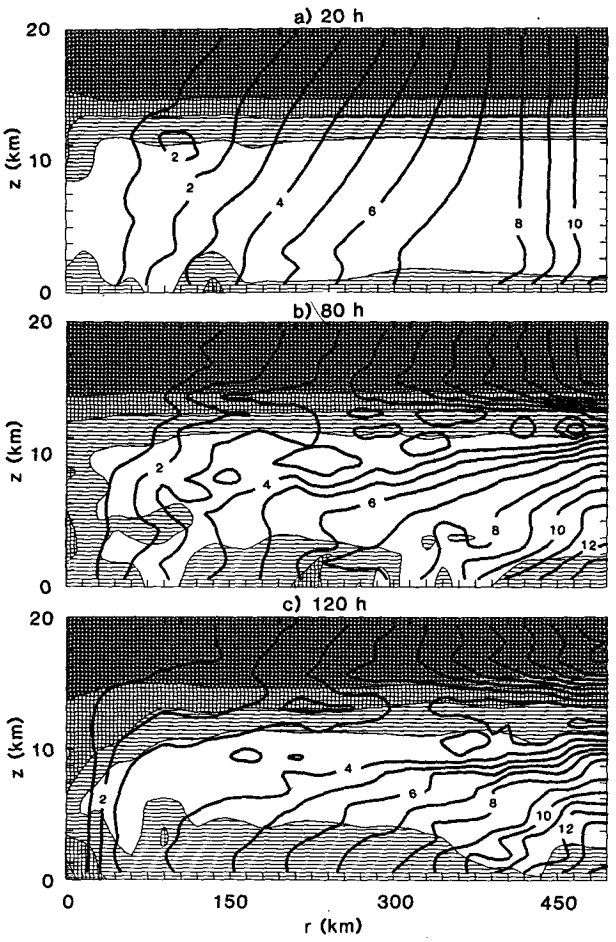

FIG. 11. θ_e^* with M surfaces superimposed for (a) $t = 20$, (b) $t = 80$ and (c) $t = 120$ h (as in Fig. 9). In (b) all the tiny "bubbles" of M are $M = 3$ contours.

b. *The θ_e budget in the boundary layer*

A theoretical problem identified in Part I can be summarized as follows: observations (e.g., see Hawkins and Imbembo, 1976) show that θ_e in the hurricane boundary layer undergoes the largest increase in the vicinity of the eyewall. If boundary-layer air parcels converging toward the vortex center from large radii acquired latent heat at a normal rate from the ocean without mixing with the free atmosphere, the increase in θ_e should be far more gradual than is observed. This led in Part I to a subdivision of the boundary layer into three parts: the eye, the eyewall, and an outer region. The outer region was empirically defined to have constant relative humidity, whereas the inner regions were characterized by a balance between surface fluxes and horizontal advection. Figure 12 shows the θ_e distribution for the control experiment (averaged over 160–180 h); there is a rapid increase in θ_e from $r \approx 100$ km inward. The inward increase is slower from $r \approx 240$ km to $r \approx 100$ km, but beyond $r \approx 240$ km, there is no discernable trend but a lot of variation.

We take a closer look at the problem here by computing the time-averaged θ_e budget. As mentioned in Section 2, θ_e is not precisely conserved in the model since the model thermodynamics adheres to (11) and not (12). We write here the time-averaged terms of (11), and using the definition of d/dt we can arrive at the following approximate forms,

$$\left\langle \frac{\partial \theta_e}{\partial t} \right\rangle \approx \left\langle \frac{\partial \theta}{\partial t} + \frac{L}{c_p \pi} \frac{\partial q_v}{\partial t} \right\rangle \tag{38}$$

$$\left\langle u \frac{\partial \theta_e}{\partial r} \right\rangle \approx \left\langle u \frac{\partial \theta}{\partial r} + \frac{L}{c_p \pi} u \frac{\partial q_v}{\partial r} \right\rangle \tag{39}$$

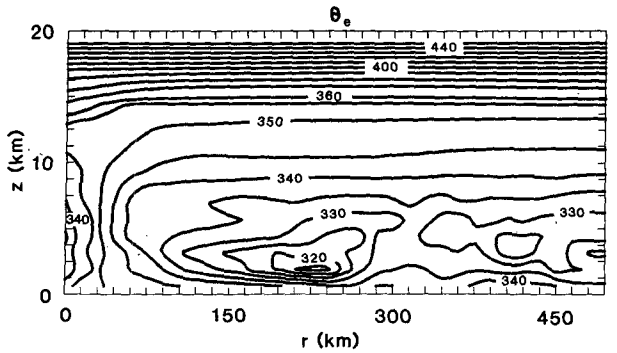

FIG. 12. θ_e for the 160–180 h average of the control experiment. Note that contour interval changes from 5 to 10 K for $\theta_e > 360$ K.

$$\left\langle w\frac{\partial\theta_e}{\partial z}\right\rangle \approx \left\langle w\frac{\partial\theta}{\partial z}+\frac{L}{c_p\pi}w\frac{\partial q_v}{\partial z}\right\rangle \tag{40}$$

$$-\left\langle\frac{1}{r}\frac{\partial rF_r^{\theta_e}}{\partial r}\right\rangle \approx -\left\langle\frac{1}{r}\frac{\partial rF_r^{\theta}}{\partial r}+\frac{L}{c_p\pi}\frac{1}{r}\frac{\partial rF_r^{q_v}}{\partial r}\right\rangle \tag{41}$$

$$-\left\langle\frac{\partial F_z^{\theta_e}}{\partial z}\right\rangle \approx -\left\langle\frac{\partial F_z^{\theta}}{\partial z}+\frac{L}{c_p\pi}\frac{\partial F_z^{q_v}}{\partial z}\right\rangle. \tag{42}$$

The averaged rate of change due to radiation is simply $\langle R\rangle$ and angle brackets denote a time average, which in the present case is taken over 20 h.

Figure 13 shows the results of taking 20-h average of the terms in (11) at $z = \Delta z/2$ (625 m) over the period 170–190 h (this period was slightly more steady than the 160–180 h period used in computing the averaged fields for the control run). Within $r \approx 240$ km the tendency is negligible, and we have a truly steady flow; the heating due to the sea-surface transfer is balanced by the cooling due to the inward advection. Beyond $r \approx 240$ km, however, Fig. 13 shows that the flow is not steady, consistent with the mature state physics described by Ooyama (1982). Examination of the model data shows that in that outer region there is a continual cycle of convection and precipitation so that at any radius, θ_e will vary with time so that the average of the tendency will always give the difference between starting and ending values of θ_e for the averaging period and will not necessarily be zero. However, inspection of the model data also gives the impression that the highs and lows of $\langle\theta_e\rangle$ from $r \approx 240$ km outward would average to a time-independent constant. To quantify this notion we take the areal average of the terms in (38)–(40) from $r \approx 240$ km to $r \approx 1125$ km (beyond this radius convection had not yet started by 190 h). We let

$$\overline{(\ )}^A \equiv \frac{2\pi}{\text{Area}}\int(\ )rdr.$$

At the lowest grid level for $\theta_e(\Delta z/2)$ it is easy to show that

$$\bar\rho\Delta z\left\langle\overline{u\frac{\partial\theta_e}{\partial r}}+\overline{w\frac{\partial\theta_e}{\partial z}}\right\rangle^A\Bigg|_{\Delta z/2} \approx \bar\rho\overline{\langle w\theta_e\rangle}^A|_{\Delta z}, \tag{43}$$

since the radial fluxes at the inner and outer limits of the region are negligible. Similarly, the areal average of the turbulent diffusion is

$$\overline{\langle F_z^{\theta_e}\rangle}^A|_{\text{surf}} - \overline{\langle F_z^{\theta_e}\rangle}^A|_{\Delta z}.$$

The budget analysis shows that the second of these and the areally averaged tendency,

$$\overline{\left\langle\frac{\partial\theta_e}{\partial t}\right\rangle}^A,$$

are negligible so that

$$c_p\bar\rho\overline{\langle w\theta_e\rangle}^A|_{\Delta z} \approx c_p\bar\rho\overline{\langle F_z^{\theta_e}\rangle}^A|_{\text{surf}} \approx 50\,\text{W m}^{-2}. \tag{44}$$

That is, the latent heat flux from the sea surface is balanced by the explicitly calculated latent heat flux to the free atmosphere. We can further refine this result by asking what part of the areally averaged flux is carried by the time-mean circulation and what part by the fluctuations in space and time. Accordingly, we compute

$$c_p\bar\rho\overline{\langle w\rangle\langle\theta_e\rangle}^A|_{\Delta z} \approx 10\,\text{W m}^{-2}.$$

The time-mean circulation accounts for approximately 20% of the total flux, and so we may conclude that the latent heat flux from the sea surface is essentially balanced by the model cumulus cloud's transport of latent

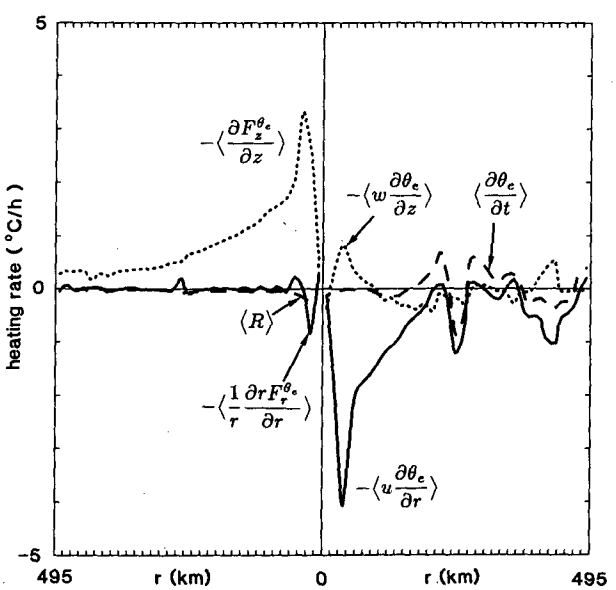

FIG. 13. Terms in time-averaged θ_e budget at $z = \Delta z/2$ (625 m). See text for explanation.

heat upwards (actually low-θ_e air downwards) in the outer region of the vortex.

In the region from $r \approx 240$ km inwards the time-mean circulation is dominant. Figure 14 displays the sensible and latent components of the horizontal advection and vertical flux convergence of θ_e, respectively. Owing to the extreme stability (see Fig. 5) above the boundary layer from $r \approx 75$ km outward to $r \approx 240$ km, the turbulent flux convergence there reflects the transfer of latent and sensible heat at the sea-surface, i.e., $\langle F_z^{\theta_e} \rangle|_{\Delta z} \approx 0$. Therefore, Fig. 14 shows that in this region the flux of moist entropy from the sea surface is dominated by latent heat transfer while the turbulent flux of sensible heat flux is small and slightly negative, as found in previous studies (cf. Anthes and Chang, 1978). In the eyewall region where turbulent mixing is greatest, the sensible heat flux convergence is positive *due to downward mixing of high-θ air.* Similarly, the flux of q_v from the sea surface is overwhelmed by the mixing of dryer air downward so that the flux convergence is negative. However, the combined effect is positive as shown in Fig. 13. The innermost region represents the boundary layer beneath the model-equivalent eye; Fig. 13 shows that only the turbulent vertical flux convergence tends to heat this point and all other terms (most notably the radiation term) are cooling.

We look at the variation of θ, T, θ_e, q_v and RH along $z = \Delta z/2$ in Fig. 15. The radial variation in θ_e may be thought of as being composed of three parts (if T = constant which Fig. 15 shows is nearly true),

$$\Delta\theta_e = \Delta\theta + \frac{L}{c_p\pi}\mathrm{RH}\Delta q_{vs} + \frac{L}{c_p\pi}q_{vs}\Delta\mathrm{RH}. \qquad (45)$$

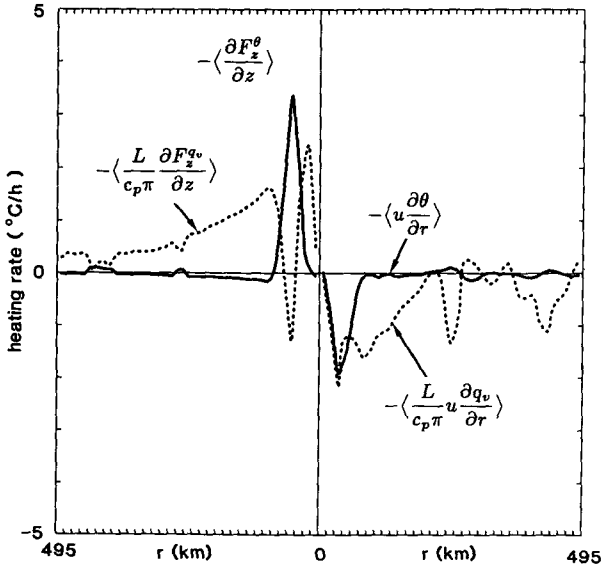

FIG. 14. Sensible- and latent-heat contributions to the radial advection and turbulent diffusion terms in the time-averaged θ_e budget shown in Fig. 12.

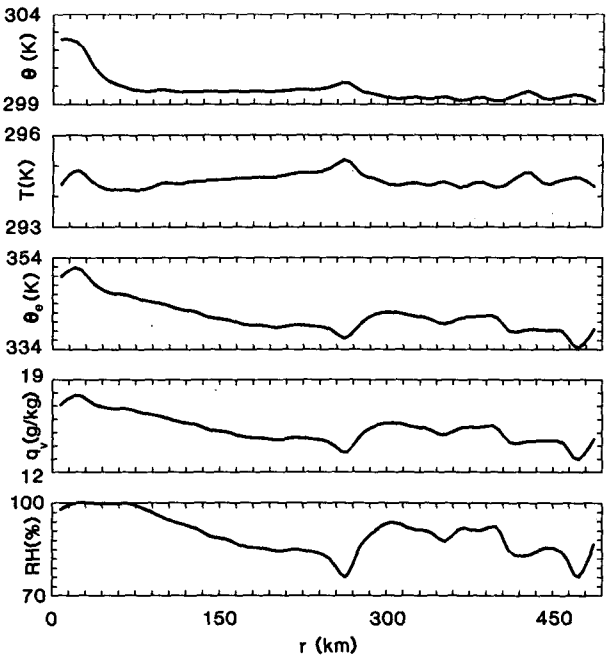

FIG. 15. θ, T, θ_e, q_v and RH vs radius at $z = \Delta z/2 = 625$ m for the 160–180 h averaged control run.

The first and second terms are those due to *isothermal expansion;* as the air spirals inward toward low pressure at constant temperature, θ and q_{vs} increase. The last term is that part of the increase in θ_e in addition to that due to isothermal expansion. It is argued in Part I that isothermal expansion by itself could not provide a large enough increase in θ_e to support an intense cyclone. From Fig. 15, one may compute the increase in θ_e between $r = 150$ km and $r = 20$ km as

$$\Delta\theta_e \approx 11.6 = 2.8 + 2.1 + 6.7\,\mathrm{K},$$

where the numbers on the rhs correspond to the terms on the rhs in (45). Thus, latent heat transfer beyond that due to isothermal expansion is responsible for more than half the inward increase in θ_e.

c. *The θ_e budget in the outflow layer*

Figure 16 displays the terms (38)–(42) in the outflow layer. In the eyewall region, the advection of lower-θ_e air from below is balanced by outward advection of θ_e. In the outer regions, vertical advection tends to warm the atmosphere and is balanced by outward advection and radiative cooling. The radiative cooling is approximately 2 K d^{-1} and is roughly similar to observed values (e.g., see Anthes, 1982, p. 87). The balance in the eye itself is also between subsidence warming and radiative cooling. However, as discussed in section 3e, this cooling is too large, and so the temperature is not as large as it should be (see Fig. 8).

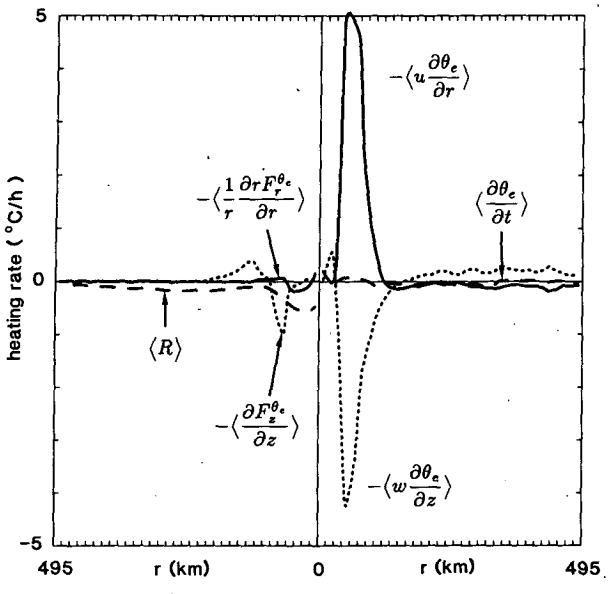

FIG. 16. Terms in time-averaged θ_e budget in the outflow layer ($z = 8.5\Delta z = 11.625$ m).

d. *The Carnot cycle*

Figure 17 shows a trajectory of an air parcel moving through the 160–180 h averaged control run superimposed on θ_e and T. Arbitrarily starting a hypothetical journey moving with an air parcel from the position marked by a star we observe the following: moving inward along the lower surface to the place where the parcel turns and ascends, the parcel acquires the amount of heat,

$$Q_{\text{in}} = c_p T_B \ln\frac{\theta_{ec}}{\theta_{ea}},$$

where θ_{ec} is the equivalent potential temperature near the center. The parcel rises upward and flows outward moist adiabatically ($\theta_e = \theta_{ec}$) until it reaches large radii and begins its slow but ineluctable descent. Here, adiabatic warming is balanced by radiative cooling; the net heat loss found when the parcel reaches the level of θ_{ea} is

$$Q_{\text{out}} = c_p \int_{\ln\theta_{ec}}^{\ln\theta_{ea}} T d(\ln\theta_e).$$

The difference $Q_{\text{in}} + Q_{\text{out}}$ is the energy available to drive the cyclone. On the final leg of its trip, the parcel continues its downward journey and continues to lose heat. Since θ_e goes through a minimum and then increases as T increases, the parcel gains somewhat more heat than it loses; thus $Q > 0$ on this final leg. This is somewhat different from the pure Carnot cycle which has adiabatic compression ($Q = 0$) along the final leg. We note that deep convection in the normal tropical atmosphere will ascend to approximately the level where $\theta_e = \theta_{ea}$; the subsiding air surrounding these clouds will follow a thermodynamic path similar to the path followed by parcels descending along the final leg of the trajectory described above. We thus believe that the small amount of net heating in the final leg is used to overcome internal dissipation within the cumuli.

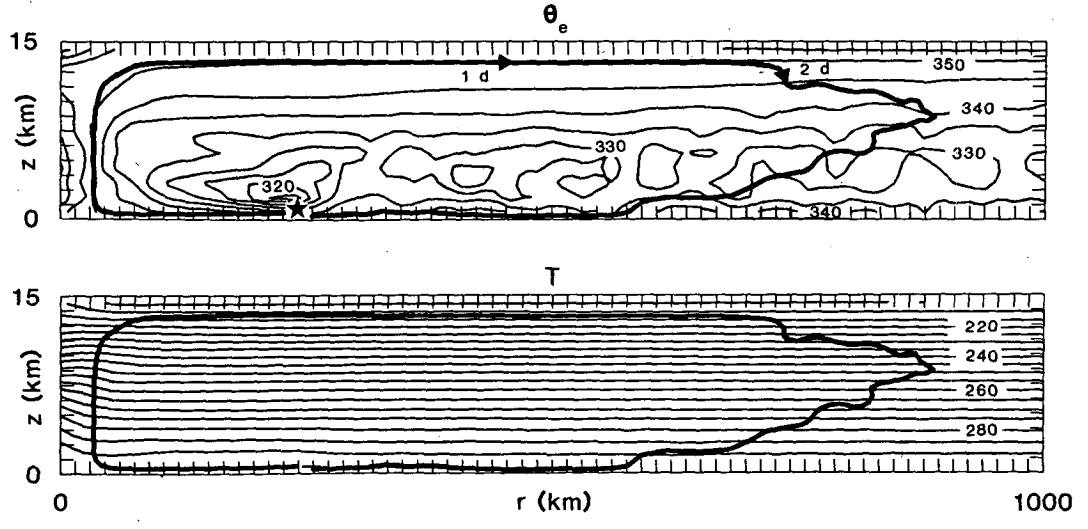

FIG. 17. An air-parcel trajectory through the eyewall, outflow layer, descent at large radius and return, superimposed on θ_e and T in the 160–180 h averaged control run. The starting point (star) is chosen where θ_e begins its steady inward increase ($\theta_e \approx 340$ K); heat is acquired at constant temperature along the sea surface; the parcel rises moist adiabatically (θ_e = constant) and eventually descends and reaches its original value of θ_e, thus losing its heat near the low-temperature tropopause. It takes approximately 40 d for the parcel to complete its journey back to the starting point over which time it acquires a small amount of extra heat which, we argue, it needs to overcome dissipation within cumulus clouds.

5. Summary

We have established, using a numerical model, that a hurricane-like vortex may grow as a result of a finite-amplitude instability in an atmosphere which is neutrally stable to the model's moist convection. The mechanism, which is a form of air–sea interaction instability, operates in such a way that wind-induced latent heat fluxes from the ocean lead to locally enhanced values of θ_e in the boundary layer which, after being redistributed upward along angular momentum surfaces, lead to temperature perturbations aloft. These temperature perturbations enhance the storm's circulation, which further increases the wind-induced surface fluxes, and so on. The tropical cyclone will continue to intensify so long as boundary-layer processes permit steadily increasing values of θ_e near the core or until the boundary layer there becomes saturated.

This view differs fundamentally from the concept of CISK as forwarded by Charney and Eliassen (1964) in that CISK emphasizes the spatial organization of the *conversion* of latent to sensible heat by cumulus convection, whereas we assert that the actual addition of total heat from the ocean drives the heat engine. Stated in another way, CISK is concerned with the spatial organization of the heating, whereas it is the correlation of heating and temperature perturbations that results in energy production. We remark that, in general, elevation of boundary-layer θ_e is necessary to generate temperature perturbations aloft; thus no amount of heating resulting purely from moisture convergence will intensify the circulation. In our view, cumulus clouds are agents for transferring heat acquired at the oceanic heat source to the upper tropospheric heat sink. This view is summarized in Fig. 18 which shows the total change of θ_e^* aloft, and θ_e at the lowest grid point, along angular momentum surfaces between the initial time and a 20-hour average during the mature quasi-steady phase. The change of θ_e^* aloft is less than or equal to the change of θ_e in the boundary layer at the base of the angular momentum surfaces, except in the eye and in the descent region at large radii, where subsidence warming leads to additional temperature changes. This shows that the warming of the vortex is strongly controlled by the boundary-layer moist-entropy budget and not by the distribution of convection per se; in the mature state the distribution of convection is controlled by Ekman-layer dynamics but has no feedback on the balanced circulation. (Were the organization of convection itself important in determining the temperature distribution in the tropical cyclone, the temperature changes along angular momentum surfaces would be largely uncoupled from changes of θ_e in the boundary layer at the bases of the angular momentum surfaces.) That convection is not perfectly effective in redistributing moist entropy upward along angular momentum surfaces is indicated by the general upward decrease of θ_e^* in Fig. 18, although this may

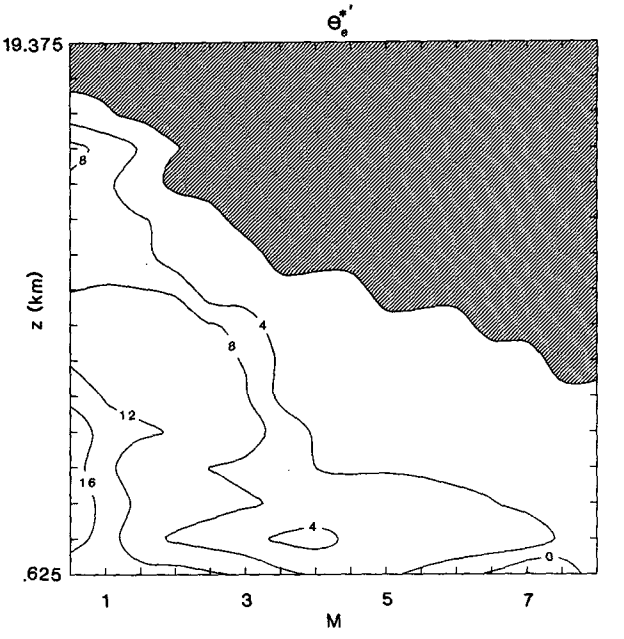

FIG. 18. The total change of $\theta_e^{*\prime} = (\theta_e^* - \bar{\theta}_e^*)$ along angular momentum surfaces between the initial state and the control run averaged between 160–180 h; the lowest grid point shows the change of θ_e instead. The abscissa shows the value of angular momentum in units defined in Fig. 9. The boundary of the shaded region indicates the maximum vertical displacement of angular momentum surfaces.

be partially attributable to the lack of exact conservation of θ_e defined by (12).

In Part I it was argued that the tropical cyclone is a Carnot engine operating with an efficiency that reflects the difference between the temperature at the top of the mixed layer and the outflow temperature. We have tested the theoretical predictions of Part I, which are consistent with the Carnot principle, against the numerical experiments and found excellent agreement. The present work shows that the heat engine needs a finite-amplitude "starter" to begin working; this is consistent with the observation that tropical cyclones result from preexisting disturbances such as easterly waves and do not arise spontaneously, even under favorable thermodynamic and kinematic conditions. The horizontal dimensions of the starting disturbance appear to have a major effect on the size of the mature storm. We have not yet addressed the question of what factors in the initial condition determine the critical amplitude for intensification, nor are we able to examine the influence of initially nonaxisymmetric flow on the vortex development.

We confirm the essential importance of boundary-layer processes in controlling the structure and evolution of the vortex. While the inner region is characterized by a near balance between surface fluxes and advection, the surface fluxes are more nearly balanced by moist convection in the outer region. This adds support to the conjecture of Ooyama (1982) and others

that the outer region is never really steady; the vortex above the boundary layer remains unsaturated and convection continually imports low-θ_e air into the boundary layer. Our numerical model only crudely simulates many of the processes affecting the boundary-layer heat budget—we feel that a better understanding of tropical-cyclone dynamics hinges crucially on observational and theoretical investigations of sea-surface heat and momentum fluxes and of turbulent and convective heat exchange through the top of the subcloud layer.

Acknowledgments. We would like to thank Joseph Klemp for his indispensable advice on the construction of the numerical model and Paul Mason for his guidance on the turbulence parameterization. Kerry Emanuel was supported in part by NSF grants ATM-8313454 and ATM-8513871.

APPENDIX

Numerical Techniques

The time-integration technique is as described by KW (p. 1079) with the modification later used by Durran and Klemp (1983, p. 2344) and will not be repeated here. We use standard second-order conservative differences for the advection terms instead of the fourth-order nonconservative scheme of KW. Although advection of isolated disturbances (e.g., a thunderstorm) is handled poorly by second-order schemes, this is not a serious concern here. Therefore, in the present case we feel that the guaranteed conservation of the second-order scheme outweighs the gains in accuracy obtained in using the non-conservative fourth-order scheme. Following Lilly (1964) we arrive at the following conservative finite-difference forms,

$$f_u = -\frac{1}{r}\overline{\overline{ru}^{r}\delta_r u}^{r} - \frac{1}{\bar{\rho}r}\overline{\overline{\rho rw}^{r}\delta_z u}^{z} + \overline{\left(\frac{v^2}{r}+fv\right)}^{r} \tag{A1}$$

$$f_v = -\frac{1}{r}\overline{ru\delta_r v}^{r} - \frac{1}{\bar{\rho}}\overline{\rho w\delta_z u}^{z} - \left(\frac{v}{r}+f\right)\frac{\overline{ru}^{r}}{r} \tag{A2}$$

$$f_w = -\frac{1}{\bar{\rho}}\overline{\overline{\rho u}^{z}\delta_r w}^{r} - \frac{1}{\bar{\rho}}\overline{\overline{\rho w}^{z}\delta_z w}^{z} + g\left\{\frac{\bar{\theta}^{z}}{\bar{\theta}} - 1 + 0.61(\overline{q_v}^{z} - \overline{q_v}) - \overline{q_l}^{z}\right\} \tag{A3}$$

$$f_\chi = -\frac{1}{r}\overline{ru\delta_r\chi}^{r} - \frac{1}{\bar{\rho}}\overline{\rho w\delta_z\chi}^{z}, \tag{A4}$$

where

$$\bar{\psi}^{x} \equiv \frac{\psi(x+\Delta x/2)+\psi(x-\Delta x/2)}{2}$$

$$\delta_x\psi \equiv \frac{\psi(x+\Delta x/2)-\psi(x-\Delta x/2)}{\Delta x}$$

and χ denotes either θ, q_v or q_l. Here (A1)–(A4) are used in place of KW's (3.6)–(3.7).

The condensation calculation is identical to that described by KW (p. 1080) (developed by Soong and Ogura, 1972) as is the calculation of the rainfall term. The only difference is that the full pressure is used in expression $L/c_p\pi$ because departures from the mean can be large in tropical cyclones.

The calculation of the eddy viscosity ν is done at a w point, rather than at the thermodynamic point as in KW. In the present problem we anticipated that vertical turbulent transports, especially near the lower boundary, are important; and extra accuracy is obtained by having ν at a w point so that vertical fluxes such as $-\nu\partial\theta/\partial z$ can be calculated with a minimum amount of averaging (P. J. Mason, private communication, 1985). Thus, the Richardson number in finite-difference form is, if the air is unsaturated, i.e., if $q_l(z+\Delta z/2)\times q_l(z-\Delta z/2)=0$ is

$$\mathrm{Ri} = \frac{g}{\bar{\theta}_v}\delta_z\theta_v S^{-2}, \tag{A5}$$

and, if saturated,

$$\mathrm{Ri} = \{A\delta_z\theta_e - g\delta_z q_t\}S^{-2}. \tag{A6}$$

The finite-difference form of the deformation consistent with the energy equation (21) is

$$S^2 = 2\left\{\overline{(\delta_r u)^2}^{z} + \overline{\overline{\left(\frac{u}{r}\right)^{r2}}^{z}} + \overline{(\delta_z w)^2}^{z}\right\} + \overline{(\delta_z u+\delta_r w)^2}^{rz} + \overline{\left(\delta_r v - \frac{v}{r}\right)^2}^{rz} + (\delta_z v)^2. \tag{A7}$$

With (A6) and (A7), ν is calculated through (26). And with ν so calculated, the consistent form of the diffusion terms, (13)–(18), is

$$D_u = \frac{1}{r}\delta_r(r2\bar{\nu}^{z}\delta_r u) + \delta_z[\bar{\nu}^{r}(\delta_z u+\delta_r w)] - 2\bar{\nu}^{rz}\frac{u}{r^2} \tag{A8}$$

$$D_v = \frac{1}{r^2}\delta_r\left[r^2\bar{\nu}^{rz}\left(\delta_r v - \frac{v}{r}\right)\right] + \delta_z(\nu\delta_z v) \tag{A9}$$

$$D_w = \frac{1}{r}\delta_r[r\bar{\nu}^{r}(\delta_z u+\delta_r w)] + \delta_z(2\bar{\nu}^{z}\delta_z w) \tag{A10}$$

$$D_\chi = -\frac{1}{r}\delta_r(r\bar{\nu}^{rz}\delta_r\chi) - \delta_z(\nu\delta_z\chi). \tag{A11}$$

The procedure for calculating the horizontal eddy viscosity in (29) is analogous and, as discussed in section 2, is used in (A8)–(A11) in the radial fluxes in the event that $\nu < \nu_H$.

The numerical treatment of the open boundary condition (31) is as in KW (p. 1081), and we use the weak time filter described by KW to suppress the mode-

splitting tendency of the leap-frog time-integration procedure. No spatial filters were used in the present study.

REFERENCES

Anthes, R. A., 1982: *Tropical Cyclones: Their Evolution, Structure and Effects,* Meteor. Monogr. No. 41, Amer. Meteor. Soc., 208 pp.

——, and S. W. Chang, 1978: Response of the hurricane boundary layer to changes of sea-surface temperature in a numerical model. *J. Atmos. Sci.,* **35,** 1240–1255.

Arakawa, A., and W. H. Schubert, 1974: Interaction of a cumulus cloud ensemble with the large-scale environment, Part I. *J. Atmos. Sci.,* **31,** 674–701.

Bird, R. B., W. E. Stewart and E. N. Lightfoot, 1960: *Transport Phenomena.* Wiley & Sons, 780 pp.

Charney, J. G., and A. Eliassen, 1964: On the growth of the hurricane depression. *J. Atmos. Sci.,* **21,** 68–75.

Durran, D. R., and J. B. Klemp, 1983: A compressible model for the simulation moist mountain waves. *Mon. Wea. Rev.,* **111,** 2341–2361.

Dutton, J. A., 1976: *The Ceaseless Wind.* McGraw-Hill, 579 pp.

Emanuel, K. A., 1986: An air–sea interaction theory for tropical cyclones. Part I: Steady state maintenance. *J. Atmos. Sci.,* **43,** 585–604.

Fjortoft, R., 1953: On the changes in the spectral distribution of kinetic energy for two-dimensional, nondivergent flow. *Tellus,* **5,** 225–230.

Hack, J. J., and W. H. Schubert, 1981: Lateral boundary conditions for tropical cyclone models. *Mon. Wea. Rev.,* **109,** 1404–1420.

Hawkins, H. F., and S. M. Imbembo, 1976: The structure of a small, intense hurricane—Inez 1966. *Mon. Wea. Rev.,* **104,** 418–442.

Jordan, C. L., 1958: Mean soundings for the West Indies area. *J. Meteor.,* **15,** 91–97.

Klemp, J. B., and R. B. Wilhelmson, 1978: The simulation of three-dimensional convective storm dynamics. *J. Atmos. Sci.,* **35,** 1070–1096.

Kurihara, Y., 1975: Budget analysis of a tropical cyclone model simulated in a axisymmetric numerical model. *J. Atmos. Sci.,* **32,** 25–59.

——, and R. E. Tuleya, 1974: Structure of a tropical cyclone in a three-dimensional numerical simulation model. *J. Atmos. Sci.,* **31,** 893–919.

Lilly, D. K., 1962: On the numerical simulation of buoyant convection. *Tellus,* **14,** 148–172.

——, 1964: Numerical solutions for the shape-preserving two-dimensional thermal convection element. *J. Atmos. Sci.,* **21,** 83–98.

Malkus, J. S., and H. Riehl, 1960: On the dynamics and energy transformations in steady state hurricanes. *Tellus,* **12,** 1–20.

Mason, P. J., and R. I. Sykes, 1982: A two-dimensional numerical study of horizontal roll vortices in an inversion capped planetary boundary layer. *Quart. J. Roy. Meteor. Soc.,* **108,** 801–823.

Merrill, R. T., 1984: A comparison of large and small tropical cyclones. *Mon. Wea. Rev.,* **112,** 1408–1418.

Moss, M. S., and S. L. Rosenthal, 1975: On the estimation of planetary boundary layer variables in mature hurricanes. *Mon. Wea. Rev.,* **103,** 980–988.

Ooyama, K., 1969: Numerical simulation of the life-cycle of tropical cyclones. *J. Atmos. Sci.,* **26,** 3–40.

——, 1982: Conceptual evolution of the theory and modeling of the tropical cyclone. *J. Meteor. Soc. Japan,* **60,** 369–380.

Riehl, H., 1954: *Tropical Meteorology.* McGraw-Hill, 392 pp.

Rosenthal, S. L., 1978: Numerical simulation of tropical cyclone development with latent heat release by resolvable scales. I: Model description and preliminary results. *J. Atmos. Sci.,* **35,** 258–271.

Smagorinsky, J., 1963: General circulation experiments with the primitive equations. I: The basic experiment. *Mon. Wea. Rev.,* **91,** 99–164.

Soong, S.-T., and Y. Ogura, 1972: Numerical simulation of warm rain development in an axisymmetric cloud model. *J. Atmos. Sci.,* **31,** 1262–1285.

Takeda, T., 1966: The downdraft in the convective cloud and raindrops a numerical computation. *J. Meteor. Soc. Japan,* **44,** 1–11.

Yamasaki, M., 1977: A preliminary experiment of the tropical cyclone without parameterizing the effects of cumulus convection. *J. Meteor. Soc. Japan,* **55,** 11–31.

Yanai, M., 1964: Formation of Tropical Cyclones. *Rev. Geophys.,* **2,** 367–414.

Willoughby, H. E., H.-L. Jin, S. J. Lord and J. M. Piotrowicz, 1984: Hurricane structure and evolution as simulated by an axisymmetric, nonhydrostatic numerical model. *J. Atmos. Sci.,* **41,** 1169–1186.